Design of cold-formed steel columns subject to local buckling at elevated temperatures

M. Rokilan and M. Mahendran

Queensland University of Technology (QUT), Brisbane, Australia

Abstract: Cold-formed steel (CFS) is one of the popular materials in low and mid-rise building construction. However, CFS member capacities reduce at elevated temperatures as their yield strength and Young's modulus decrease with increasing temperature. In addition, CFS exhibits nonlinear stress-strain characteristics at elevated temperatures, which is significantly different to the ambient temperature stress-strain characteristics. Although several studies have been conducted on the elevated temperature local buckling capacities of CFS columns, they have not considered the effects of nonlinear stress-strain characteristics such as the nonlinearity between proportional limit stress and yield strength, varying yield-strength to Young's modulus ratio and strain hardening between yield and ultimate strengths. Thus, this research study investigated their effects in detail, and proposed modified design equations for the elevated temperature local buckling capacities of CFS columns based on the effective width and direct strength methods given in AS/NZS 4600, since the current design equations give unsafe predictions in many cases. The modified design equations incorporating the effects of elevated temperature nonlinear stress-strain characteristics were developed using the local buckling capacities of CFS columns obtained from 740 finite element models of lipped channel sections. A simplified design method is proposed to determine the compression capacities of commonly used Australian open CFS sections at elevated temperatures.

Keywords: Cold-formed steel columns; Local buckling; Elevated temperatures; Nonlinearity; Strain-hardening.

1. Introduction

Cold-formed steel (CFS) sections are extensively used in both low-rise and mid-rise constructions due to their structural, economic and environmental benefits [1]. However, their structural capacities reduce at elevated temperatures as observed for other construction materials [2]. Also, CFS sections are commonly subject to section failures caused by local buckling due to their larger width to thickness (b/t) ratio compared to hot-rolled steel sections.

Hence, it is essential to accurately determine the elevated temperature local buckling capacities of CFS columns in order to determine their period of structural adequacy in fire.

CFS columns are mainly used in light gauge steel framed (LSF) wall and floor systems. Fire resistance levels (FRL) of LSF walls and floors are based on their insulation, integrity and structural failure times. Many studies have been conducted on the FRL of LSF walls and floors. Ariyanayagam and Mahendran [3] and Steau and Mahendran [4] conducted standard fire tests to determine the insulation and integrity failure times of LSF walls and floors, respectively, while Ariyanayagam and Mahendran [2] conducted standard fire tests to determine the structural failure times of LSF walls, where CFS columns experience non-uniform temperature conditions. However, it is essential to understand the behaviour of CFS columns under uniform elevated temperature conditions before studying their behaviour under non-uniform elevated temperature conditions. Thus, this paper focuses on the local buckling behaviour of CFS columns under uniform elevated temperature conditions.

Recent research studies [5, 6] proposed the use of ambient temperature design equations in the CFS design standards together with appropriate reduction factors for elevated temperature mechanical properties to determine the local buckling capacities of CFS columns at elevated temperatures. Gunalan et al. [6] however highlighted the importance of accounting for the effects of nonlinearity of elevated temperature material properties since the capacity predictions were found to be conservative or unsafe in several cases. A comparison of the stress-strain curves of cold-formed steels (Fig. 1) shows significant differences at ambient and elevated temperatures due to varying nonlinearity levels [7]. These differences can be categorised under three areas as shown in Fig. 1, namely, nonlinearity between proportional limit stress and yield strength (n), strain hardening between yield and ultimate strengths and varying yield strength to Young's modulus ratio (e). As seen in Fig. 1, secant modulus at any point between proportional limit stress and yield strength is less than Young's modulus for nonlinear stress-strain curves while secant and Young's moduli are the same at any point up to yield strength for elastic perfect plastic (EPP) stress-strain curves. Thus, the elevated temperature local buckling capacities obtained from CFS design standards, which are based on the EPP stress-strain curves, can be unsafe. On the other hand, strain hardening may increase the local buckling capacities of CFS columns. Also, the yield strength to Young's modulus ratio is not a constant at ambient and elevated temperatures due to the differences in their elevated temperature reduction factors as shown in Fig. 1. This varying yield strength to Young's modulus ratio with increasing temperatures can influence the local buckling capacity

of CFS columns when nonlinearity is present. This is why it is included along with the nonlinearity parameter (n) and strain hardening.

Rokilan and Mahendran [8] proposed modified design methods by including the effects of nonlinearity in determining the global buckling capacities of CFS columns at elevated temperatures. The modified design methods were shown to be capable of predicting the global buckling capacities much closer to the finite element and experimental capacities. This indicates that the direct use of ambient temperature design equations without incorporating the aforesaid effects of nonlinear material characteristics is unlikely to predict the elevated temperature local buckling capacities of CFS columns accurately.

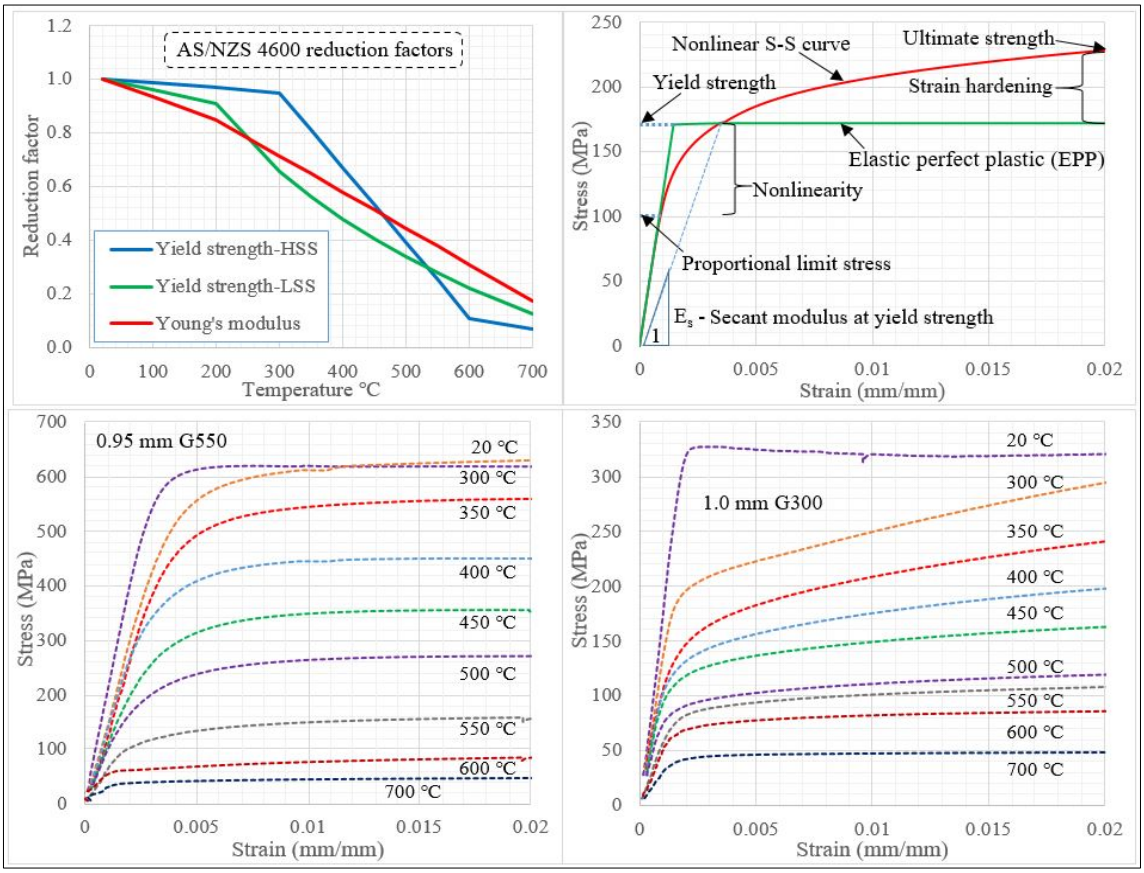

Fig. 1. AS/NZS 4600 [9] mechanical property reduction factors and stress-strain curves of cold-rolled steel sheets at ambient and elevated temperatures [7].

AS/NZS 4600 [9] recognises the effects of nonlinear stress-strain characteristics at elevated temperatures as it limits the use of its design equations if the proportional limit stress to yield strength ratio is less than 0.75. Although AS/NZS 4600 says that nonlinearity is present normally for low strength steels (LSS - yield strength less than 450 MPa), Rokilan and Mahendran [7] observed the presence of a high level of nonlinearity in both low and high

strength steels (HSS) in the temperature range of 300 to 550 ℃. Thus, AS/NZS 4600 design method cannot be used to determine the local buckling capacities of CFS columns in this critical temperature range. On the other hand, Bezkorovainy et al. [10] proposed modified ambient temperature local buckling capacity curves by incorporating a nonlinearity factor (n) and the yield strength to Young's modulus ratio (e) to take into account the effects of nonlinearity observed in the ambient temperature stress-strain curves of stainless steel. Thus, it is essential to investigate the effects of nonlinear stress-strain characteristics of CFS on the elevated temperature local buckling capacities of CFS columns and incorporate them in the design method.

In this research study, a numerical investigation of CFS columns subject to local buckling was conducted using validated finite element models in which the nonlinear elevated temperature stress-strain curves of CFS were incorporated. Following this numerical investigation of Lipped Channel Sections (LCS) made of different steel grades, two design methods were proposed by modifying the effective width and direct strength methods in AS/NZS 4600 [9] to include the effects of nonlinear stress-strain characteristics of CFS at elevated temperatures. A simplified design method was also proposed for CFS columns made of Australian open CFS sections at elevated temperatures. These modified and simplified design methods are capable of predicting the elevated temperature local buckling capacities of CFS columns with a higher degree of accuracy. Details and findings of this research study are presented in this paper.

2. Finite element model development and validation

The effects of nonlinear stress-strain characteristics on the local buckling capacity of CFS columns were investigated using a detailed finite element analysis based parametric study of short LCS columns with fixed ends. Numerical parametric study was used since it is difficult to find materials with different 'n' values, strain hardening and 'e' values. However, it is necessary to validate the developed finite element (FE) models using experimental results before the extensive use of FE models to conduct a detailed parametric study. Thus, experimental results of Gunalan et al. [6] were used in this research to validate the ABAQUS [11] FE models of lipped channel sections (LCS) at ambient and elevated temperatures up to 700 ℃. The dimensions and mechanical properties of LCS columns used for validation are given in Table 1. The experimental results used for validation in this paper were also used by Gunalan et al. [6] to validate their FE models. Thus, the same modelling parameters were used in this paper with brief explanations.

According to a recent review paper by Maraveas [16], experimental studies on the local buckling of CFS members in fire were conducted by [6, 12-15]. CFS lipped channel columns tested by Craveiro et al. [12] failed by global buckling or local-global interaction buckling at elevated temperatures while only the unlipped channel sections tested by Feng et al. [13] failed by local buckling at elevated temperatures. CFS columns tested by Craveiro et al. [14] were made of built-up sections. Although Lee's [15] lipped channel columns failed by local buckling at elevated temperatures, his test results were affected by errors in temperature and strain measurements as indicated by Ranawaka and Mahendran [17]. Hence the test results of Gunalan et al. [6] were selected in this study for the validation of FE models as they are the most suitable test results among the existing test results of CFS lipped channel section columns subject to local buckling at elevated temperatures.

2.1. Element type, mesh details and mechanical properties

CFS sections are modelled using shell elements due to their small thickness. Gunalan et al. [6] used S4 element after investigating the appropriateness of different shell elements, such as S4, S4R, S4R5 and S8R5. Thus, S4 element was used in this study. Suitable mesh sizes were chosen based on the convergence studies conducted by Gunalan et al. [6], who recommended 3 mm x 3 mm for LCS columns (Fig. 2).

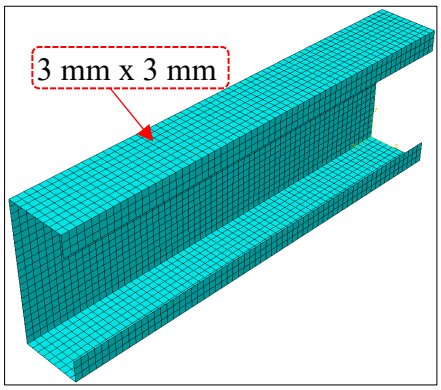

Fig. 2. Mesh details of LCS column model.

The two-stage stress-strain model (Eqs. 1 to 6) proposed by Rokilan and Mahendran [7] was used to obtain the engineering stress-strain relationships for the validation of finite element models. The engineering stress and strain values were converted to true stress and strain values before inputting the plastic stress and strain values in the ABAQUS [11] models. The measured values of yield strength, Young's modulus and ultimate strength at ambient and elevated temperatures were obtained from Gunalan et al. [6] while the ultimate strain and nonlinearity

factor were obtained from the reported experimental values of 0.95 mm G550 CFS in Rokilan and Mahendran [7]. Table 1 gives the yield strength, Young's modulus and 'n' value used in the validation of FE models.

$$\varepsilon_T = \frac{f_T}{E_T} + 0.002\left[\frac{f_T}{f_{y,T}}\right]^n \quad \text{for } f_T < f_{y,T} \tag{1}$$

$$\varepsilon_T = \frac{f_T - f_{y,T}}{E_{0.2}} + \left[\varepsilon_{u,T} - \varepsilon_{0.2,T} - \frac{f_{u,T} - f_{y,T}}{E_{0.2}}\right]\left[\frac{f_T - f_{y,T}}{f_{u,T} - f_{y,T}}\right]^m + \varepsilon_{0.2,T} \quad \text{for} \quad f_{y,T} \le f_T \le f_{u,T} \quad \text{and} \quad \varepsilon_T \le \varepsilon_{u,T} \tag{2}$$

$$\text{Where, nonlinearity factor (n)} = \frac{\ln(4)}{\ln(f_{y,T}/f_{0.05,T})} \tag{3}$$

$$\text{Strain hardening factor m for high strength steels (m)} = 1 + {3.3\, f_{Y,T}}/{f_{u,T}} \tag{4}$$

$$\text{Strain hardening factor m for low strength steels (m)} = 1 + {4.3\, f_{Y,T}}/{f_{u,T}} \tag{5}$$

$$\text{Tangent modulus of the stress-strain curve at the yield point } (E_{0.2}) = \frac{E_T}{1+0.002\, n \frac{E_T}{f_{y,T}}} \tag{6}$$

$\varepsilon_T, \varepsilon_{0.2,T}, \varepsilon_{u,T}, E_T, f_{y,T}, f_{0.05,T}, f_{u,T,}$ = strain corresponding to given stress f_T, yield strain, ultimate strain, Young's modulus, yield strength, 0.05% proof stress and ultimate strength at temperature (T), respectively.

2.2. Loading and end support conditions

Elastic buckling and ultimate capacities of columns depend on accurate simulation of boundary conditions. The nodes of the section at each end were tied together to a reference node at the centroid of the CFS section using a rigid fixed MPC (multi-point constraint) for the application of the boundary conditions to the column. All three displacement and rotational degrees of freedom (DOFs) at each reference node were set to zero (0) excluding the displacement DOF along Z-axis of the reference node at the loading end, which was released to allow the displacement during load application. Also, the load was assigned to the centroid of the section (Fig. 3). X, Y and Z displacement restraints are denoted by 1, 2 and 3 while X, Y and Z rotational restraints are denoted by 4, 5 and 6 in Fig. 3.

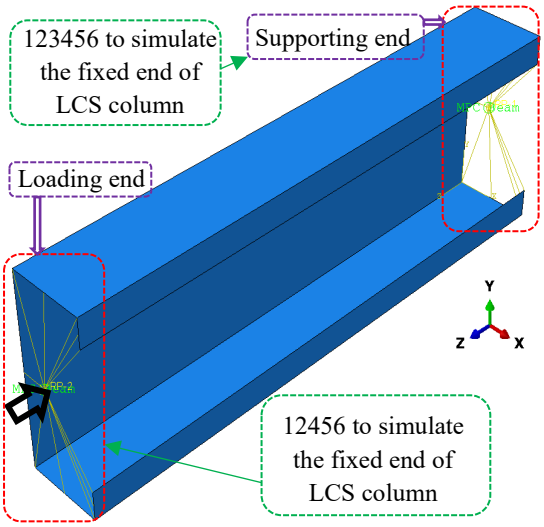

Fig. 3. Boundary conditions of fixed-ended LCS column.

2.3. Initial geometric imperfections and residual stresses

Geometric imperfections are introduced in CFS sections, mainly during their production and transportation phases. It is necessary to incorporate appropriate geometric imperfections in FE models since they significantly affect the ultimate capacity of CFS sections. In this study, cross-section geometric imperfection relevant to local buckling was considered as it focuses on the local buckling of CFS sections. Schafer and Peköz [18] proposed two different equations for the initial geometric imperfection of LCS, 0.006b, where b is the width of the web, and $6te^{-2t}$, where t is the thickness of the section. The latter was used for the validation of FE models in this study as recommended by Gunalan et al. [6]. However, it is important to consider the initial local geometric imperfection given in the CFS design standards for the parametric study since design capacity equations are proposed based on the parametric study. Therefore, the local geometric imperfection (Eq. 7) given in AS/NZS 4600 [9] was used in the parametric study.

$$\text{Local imperfection} = 0.3t\sqrt{\sigma_{0.2}/\sigma_{cr}} \tag{7}$$

where, t is the section thickness and $\sigma_{0.2}$ and σ_{cr} are yield strength and critical local buckling stress of the section determined using ABAQUS [11], respectively.

Bending and membrane residual stresses could be imparted on CFS members during cold-forming and welding processes. Membrane residual stresses, which are usually small in magnitude, are present in the corners of LCS where a higher yield strength is observed. To simplify modelling, it is often assumed that these effects compensate each other and are

neglected in numerical analyses [18]. The effect of bending residual stresses is included in the stress-strain behaviour of the material if the coupons are not straightened by plastic bending prior to testing as shown by Gardner and Cruise [19]. Also, Gunalan et al. [6] showed that the effect of bending residual stresses on the ultimate capacities of LCS columns subject to local buckling was less than 1%. Hence, both bending and membrane residual stresses were not explicitly modelled in this study.

2.4. Validation of finite element models

Finite element models were created using the ABAQUS [11] software. They were validated using the experimental results from previous research study [6]. Linear buckling analyses were conducted using the developed models to obtain the critical buckling modes which were then used to assign initial local geometric imperfections. A non-linear analysis employing the modified Riks solver was subsequently conducted to obtain the ultimate capacities. A comparison of experimental ultimate capacities and FEA predictions is shown in Table 1. The obtained mean and COV values shown in the table provide evidence that the developed FE models have the capability to produce accurate ultimate capacity results of LCS stub columns. Typical column failure mode due to local buckling as observed in tests and FE analyses are shown in Fig. 4, which also compares the load-displacement curves.

Table 1. Comparison of ultimate capacities of G550 LCS columns from tests and FEA.

Temp. (°C)	t (mm)	Web (mm)	Flange (mm)	Lip (mm)	Yield strength (MPa)	Young's modulus (MPa)	'n' value	FEA (kN)	Test (kN)	$\frac{\text{Test}}{\text{FEA}}$
20	0.95	62.0	26.7	9.2	615	205000	16	52.9	53.9	1.02
200	0.95	62.4	26.8	9.2	609	174189	15	51.5	52.1	1.01
300	0.95	62.3	26.7	9.1	584	146596	8	46.6	47.8	1.03
400	0.95	62.4	26.7	9.2	427	118921	7	35.1	36.4	1.04
500	0.95	62.6	26.8	9.2	240	911246	6	20.7	21.4	1.04
600	0.95	62.1	26.8	9.2	68	63571	30	6.7	6.6	0.99
700	0.95	62.6	26.6	9.2	43	35896	18	4.2	4.0	0.96
Mean										1.01
COV										0.03

Note: LCS column length = 190 mm

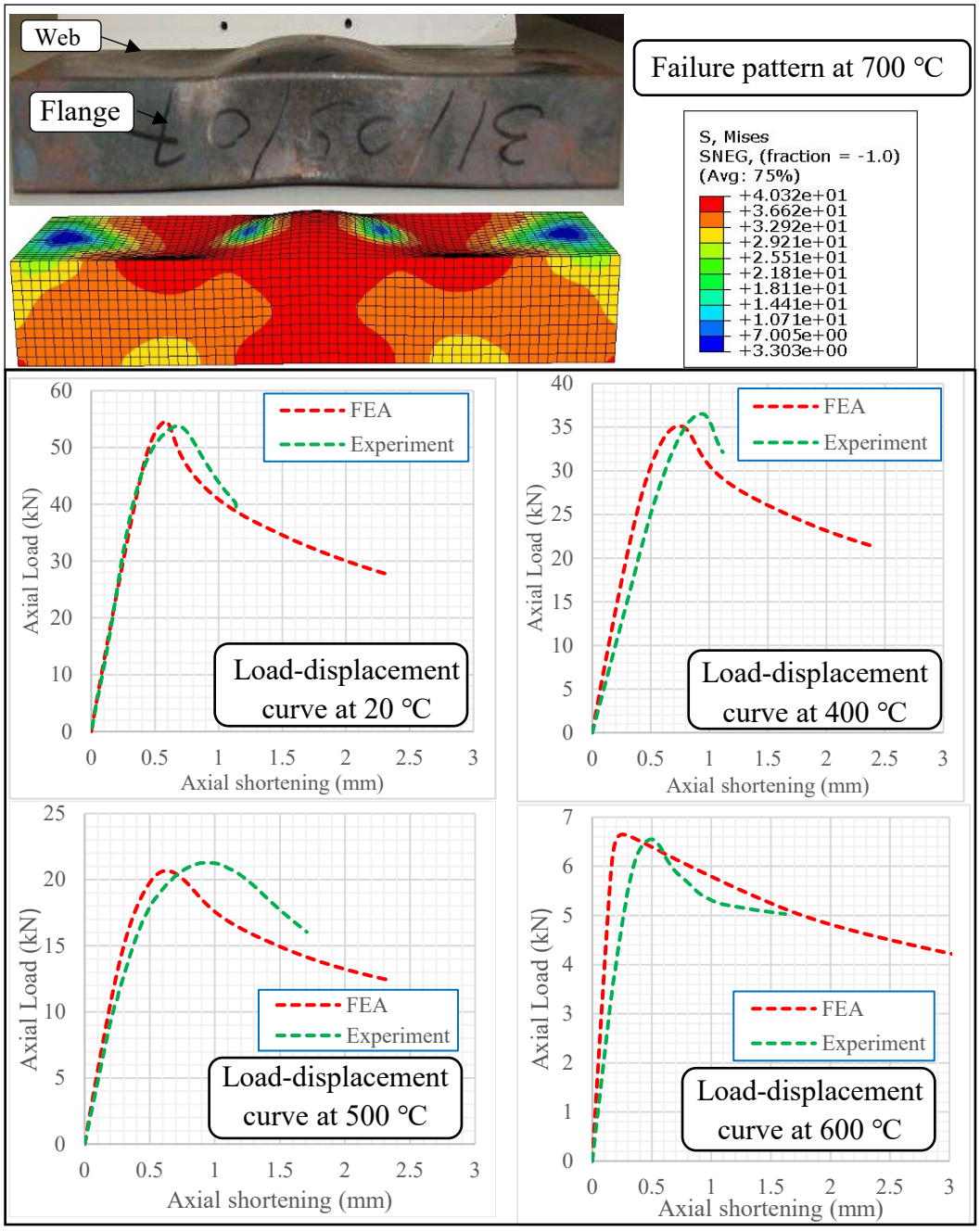

Fig. 4. Comparison of column failure modes and load-displacement curves from tests and FEA.

2.5. Details of the parametric study

Following the validation, nonlinear FE analyses of LCS columns subject to local buckling were conducted in a detailed parametric study to determine the ultimate compression capacities of LCS columns listed in Tables 2 and 3. Since the focus of this research is to investigate the effects of nonlinear stress-strain characteristics, these FE analyses have to be conducted for CFS with a large range of nonlinear stress-strain characteristics. For this purpose, it is possible to construct the nonlinear stress-strain curves of CFS using either the measured elevated

temperature properties or the idealized 'n' and 'e' factors together with different strain hardening properties (f_u and ε_u). However, elevated temperature mechanical properties of CFS vary based on the origin, steel grade and section type of the CFS, and this is evident from the varying elevated temperature mechanical properties reported in many research papers and design standards from different parts of the world. Table 4 also shows that the 'n' and 'e' values of high and low strength CFS are different at a given temperature. Therefore, the design capacity equations proposed based on the measured elevated temperature properties such as those in Table 4 can only be applied to a certain group of CFS. On the other hand, suitable design capacity equations can be proposed based on the fundamental nonlinear stress-strain parameters such as 'n' and 'e' factors and strain hardening parameters (f_u and ε_u). However, their applicability may still be limited to a narrow range of 'n' and 'e' factors, and it is difficult to study the individual effects of each parameter on the ultimate compression capacities of CFS columns. Thus, initially, idealized 'n' and 'e' factors were used together with different strain hardening properties (f_u and ε_u). The selected nonlinear stress-strain parameters cover the possible nonlinear stress-strain characteristics observed at elevated temperatures for commonly used CFS (Table 4).

Table 4 gives the elevated temperature nonlinearity factor (n), yield strength (f_y) (0.2% proof stress), ultimate strength (f_u), Young's modulus (E), ultimate strain (ε_u), yield strength to Young's modulus ratio (e), stress at 2% total strain to yield strength ratio ($f_{2\%}/f_y$) and ultimate stress to yield strength ratio (f_u/f_y) of two typical high and low strength open CFS sections used in Australia. Elevated temperature yield strength, ultimate strength and Young's modulus were calculated using the AS/NZS 4600 [9] elevated temperature reduction factors derived based on detailed experimental studies [7] while the ultimate strains are the average values recommended in Rokilan and Mahendran [7]. The 'n' factors of CFS with different thicknesses were calculated using the 0.05% proof stress and yield strength reported in Rokilan and Mahendran [7], and the minimum 'n' factor was selected at each temperature. Also, the $f_{2\%}/f_y$ ratios are for 0.95 mm G550 and 1.0 mm G300 CFS.

Two different types of LCS were used in the parametric study: LCS with one slender element (web) (Table 2); LCS with all slender elements (Table 3). AS/NZS 4600 [9] effective width method was used to determine whether the plate elements of LCS are slender. Thus, the LCS column length was selected as three times the critical local buckling half wavelength obtained from the finite strip buckling analysis software, CUFSM, to eliminate the influence of end support conditions. Also, the fixed-ended short columns used in this study avoided any

interaction with other buckling modes. The ultimate compression capacities, elastic buckling capacities and other relevant results are given in the supplementary data section of this paper.

Table 2. LCS columns with one slender element (web) used in the parametric study.

Grade	Thickness (mm)	Flange (mm)	Lip (mm)	Web width (mm)
G250	1.95	40	15	80, 100, 130, 160, 200, 250, 300
	1.15	24	9	60*, 80*, 100*, 130*, 160*, 200*
	0.95	20	7.5	40, 60, 80, 100, 130, 160
	0.75	20	8	40, 60, 80, 100
G450	1.15	24	9	40, 60, 80, 100, 130, 160
G550	1.15	24	9	40, 60*, 80*, 100*, 130*, 160*
G150	1.15	24	9	60, 80, 100, 130, 160, 200

Note: * - sections used to study strain hardening effects

Table 3. LCS columns with all slender elements used in the parametric study.

Grade	Thickness (mm)	Flange (mm)	Lip (mm)	Web width (mm)
G250	1.15	40	15	60, 80, 100, 130, 160, 200
	0.95	40	15	40, 60, 80, 100, 130, 160, 200
	0.55	40	15	40, 60, 80, 100
G450	1.15	40	15	40, 60, 80, 100, 130, 160
G550	1.15	40	15	40*, 60*, 80*, 100*, 130*, 160
	0.75	40	15	40, 60, 80, 100

Note: * - sections used to study strain hardening effects

The effects of varying stress-strain characteristics of CFS at ambient and elevated temperatures on the local buckling capacities of CFS columns were investigated under three categories, namely, nonlinearity between proportional limit stress and yield strength (n), strain hardening between yield and ultimate strengths and varying yield strength to Young's modulus ratio (e).

2.5.1. Nonlinearity between proportional limit stress and yield strength

In this case, the nonlinearity factor (n) in the two-stage stress-strain model (Eqs. 1 to 6) proposed by Rokilan and Mahendran [7] was varied in the range of 3 to 100 (3, 4, 5, 7, 9, 11, 15, 25 and 100) (Fig. 5). A lower n value signifies a higher degree of nonlinearity as evident from Fig. 5. The effects of strain hardening were minimised by maintaining a low level of strain hardening. However, due to the practical impossibility of obtaining a stress-strain relationship

without strain hardening effects, i.e. by using an ultimate to yield strength ratio (f_u/f_y) of 1.0, the ultimate to yield strength ratio and ultimate strain were chosen as 1.04 and 0.2, respectively, in the analyses. In addition to the nonlinear stress-strain models, an elastic perfect plastic (EPP) stress-strain model was also used.

For the LCS columns in Tables 2 and 3, Young's modulus of 200,000 MPa was used with yield strengths of 150, 250, 450 and 550 MPa for G150, G250, G450 and G550 steels, respectively. Ten different stress-strain curves (ten different 'n' factors) were used with 41 LCS columns with one slender element (web) (Table 2) and 33 LCS columns with all slender elements (Table 3), which produced 740 ultimate compression capacities. These ultimate compression capacities were used to investigate the accuracy of current design equations.

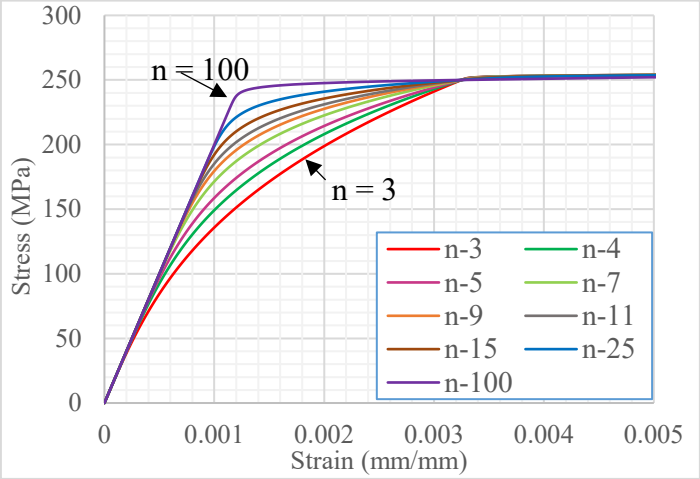

Fig. 5. Stress-strain curves used to investigate the effects of nonlinearity.

2.5.2. Yield strength to Young's modulus ratio (e)

To investigate the effects of 'e', the ultimate compression capacities of 1.15 mm G150, G250, G450 and G550 LCS columns with one slender element (web) and 1.15 mm G250, G450 and G550 LCS columns with all slender elements obtained from the above investigation were used. Although G150 steel (yield strength of 150 MPa) is not a standard grade, it was selected to investigate the effect of smaller 'e' values. The 'e' values of 150, 250, 450 and 550 MPa are 0.00075, 0.00125, 0.00225 and 0.00275, respectively.

2.5.3. Strain hardening between yield and ultimate strengths (f_u/f_y)

In this case, the ultimate to yield strength ratio (f_u/f_y) was varied from 1.04 to 1.4 together with different levels of nonlinearity (n=3 and 9) while keeping the ultimate strain constant at 0.02

(Fig. 6). The slope of the strain hardening portion is important than f_u/f_y ratio when the material parameters are selected for the strain hardening portion. For example, low strength CFS exhibits f_u/f_y ratio of 1.99 and ultimate strain of 0.22 at 350 °C while high strength CFS exhibits f_u/f_y ratio of 1.18 and ultimate strain of 0.02 at 500 °C. However, it is unlikely that CFS columns will experience a high strain such as 0.22 before they reach their ultimate capacity. Hence, the stress at 2% total strain to yield strength ratio was taken into account in the selection of f_u/f_y ratios with the ultimate strain of 0.02. The selected LCS columns are: G250-1.15 mm (6 different cross-sections) and G550-1.15 mm (5 different cross-sections) LCS with one slender element (web) (Table 2); G550-1.15 mm (5 different cross-sections) LCS with all slender elements (Table 3). Five different f_u/f_y ratios (1.04, 1.1, 1.2, 1.3 and 1.4) and two different 'n' factors (n = 3 and 9) resulted in 10 different nonlinear stress-strain curves for each CFS column, and thus, a total of 160 ultimate compression capacities.

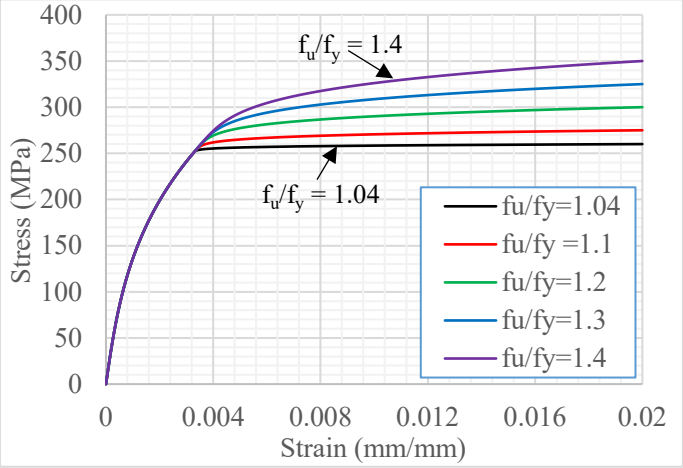

Fig. 6. Stress-strain curves of G250 steel with a nonlinearity factor of 3 and varying levels of strain hardening.

Finally, the modified design equations, which were developed based on the idealised nonlinear stress-strain curves, were further simplified for the Australian open CFS sections using their measured elevated temperature stress-strain curves. For this purpose, 1.15 mm G550 and G250 LCS column (b = 60, 80, 100, 130 and 160 mm) with one slender element (web) (Table 2) were analysed using 10 different stress-strain curves (20 to 700 °C) developed based on the parameters given in Table 4 and Eqs. 1 to 6 based on the two-stage stress-strain model in [7]. These ultimate compression capacities were used to propose a simplified design method for the Australian open CFS sections in Section 5.

Table 4. Elevated temperature mechanical properties of high and low strength CFS steel [7].

Temp. (°C)	High strength cold-formed steel (G550)								Low strength cold-formed steel (G250)							
	n	f_y	f_u	E	ε_u	e	$f_{2\%}/f_y$	f_u/f_y	n	f_y	f_u	E	ε_u	e	$f_{2\%}/f_y$	f_u/f_y
20	16	550	550	200000	0.02	0.00275	1.01	1.00	EPP	250	320	200000	0.21	0.00125	1.00	1.28
200	15	532	583	169940	0.04	0.00313	1.04	1.09	EPP	227	386	169940	0.14	0.00134	1.05	1.70
300	8	523	526	143020	0.04	0.00365	1.10	1.01	17	164	322	143020	0.18	0.00115	1.37	1.96
350	8	446	473	129520	0.03	0.00344	1.10	1.06	7	140	280	129520	0.22	0.00108	1.42	1.99
400	6	369	399	116020	0.02	0.00318	1.11	1.08	8	119	233	116020	0.18	0.00103	1.35	1.95
450	6	292	311	102520	0.02	0.00284	1.08	1.07	8	101	186	102520	0.19	0.00098	1.27	1.84
500	6	215	222	89020	0.02	0.00241	1.18	1.03	8	84	142	89020	0.19	0.00095	1.23	1.69
550	7	138	146	75520	0.06	0.00182	1.24	1.06	11	69	105	75520	0.18	0.00092	1.22	1.51
600	20	61	90	62020	0.15	0.00098	1.29	1.49	11	56	75	62020	0.16	0.00090	1.17	1.35
700	18	39	46	35020	0.07	0.00110	1.16	1.18	10	31	36	35020	0.05	0.00089	1.08	1.16

3. Effects of nonlinear stress-strain characteristics on the elevated temperature capacities of CFS columns

In this section, the ultimate compression capacities of CFS columns obtained from the numerical parametric study are evaluated. The results are plotted as either the ratio of ultimate compression capacities obtained based on the nonlinear stress-strain model and elastic perfect plastic (EPP) model versus non-dimensional section slenderness, λ_l, or the ratio of ultimate compression capacity to yield capacity versus λ_l, defined as $\sqrt{N_y/N_{ol}}$, where N_y and N_{ol} are the yield and elastic local buckling capacities, respectively.

3.1. Effects of nonlinearity and varying yield strength to Young's modulus ratio

Fig. 7 shows that the local buckling capacity of CFS columns reduces (capacity ratio reduces from 1 to 0.78) as the nonlinearity increases (EPP model to 'n' value of 3). Bezkorovainy et al. [10] also observed the same behaviour for stainless steel plates. Rokilan and Mahendran [8] highlighted that the effects of nonlinearity on the global buckling capacity are high for columns with intermediate column slenderness whereas columns with low and high column slenderness experience reduced effects for both LCS and SHS columns. However, the effects of nonlinearity on the local buckling capacity do not show a consistent relationship with changing section slenderness (λ_l) (ratios of 0.78 to 1.0 in Fig. 7). Local buckling capacity of CFS section depends on both elastic buckling and post-buckling behaviour unlike global buckling capacity which mainly depends on the elastic buckling behaviour. Also, the local buckling capacity depends on the slenderness of individual elements (element slenderness). These may be the reasons for the observed inconsistent relationship with changing λ_l. However, the effects of nonlinearity increase with increasing section slenderness for LCS with only one slender element (web) when the sizes of the non-slender flange and lip elements are unchanged (Fig. 7 (a)). Another notable observation is that the effects of nonlinearity on the local buckling capacity are considerably small in comparison with those observed for global buckling [8].

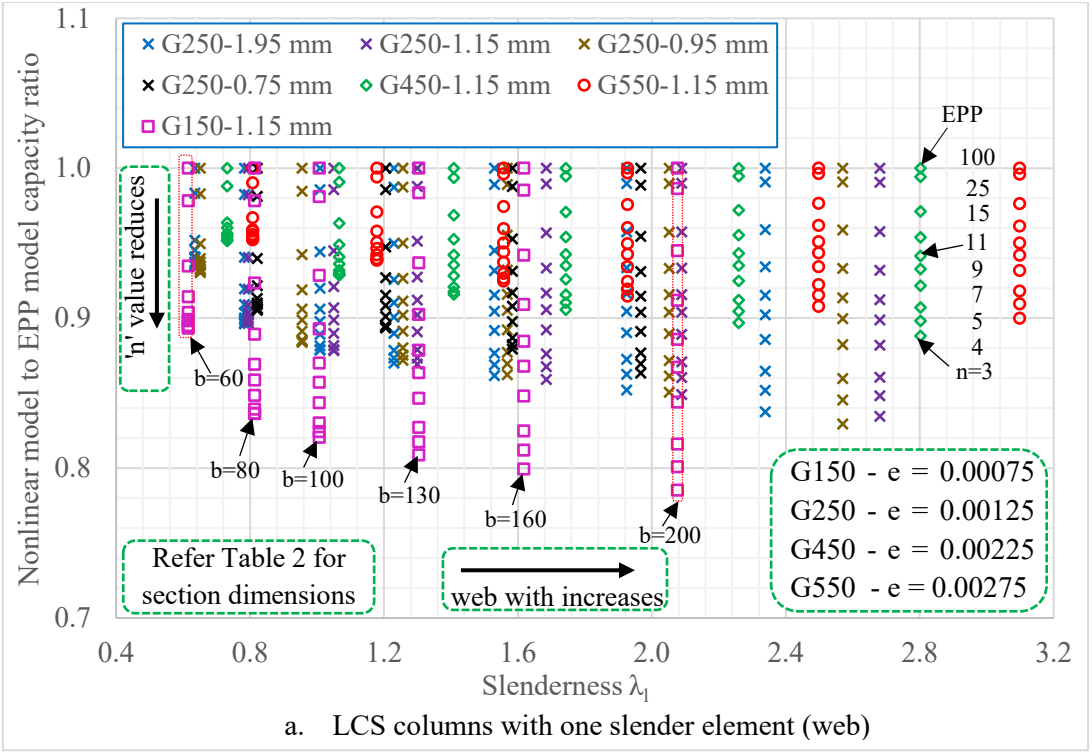

a. LCS columns with one slender element (web)

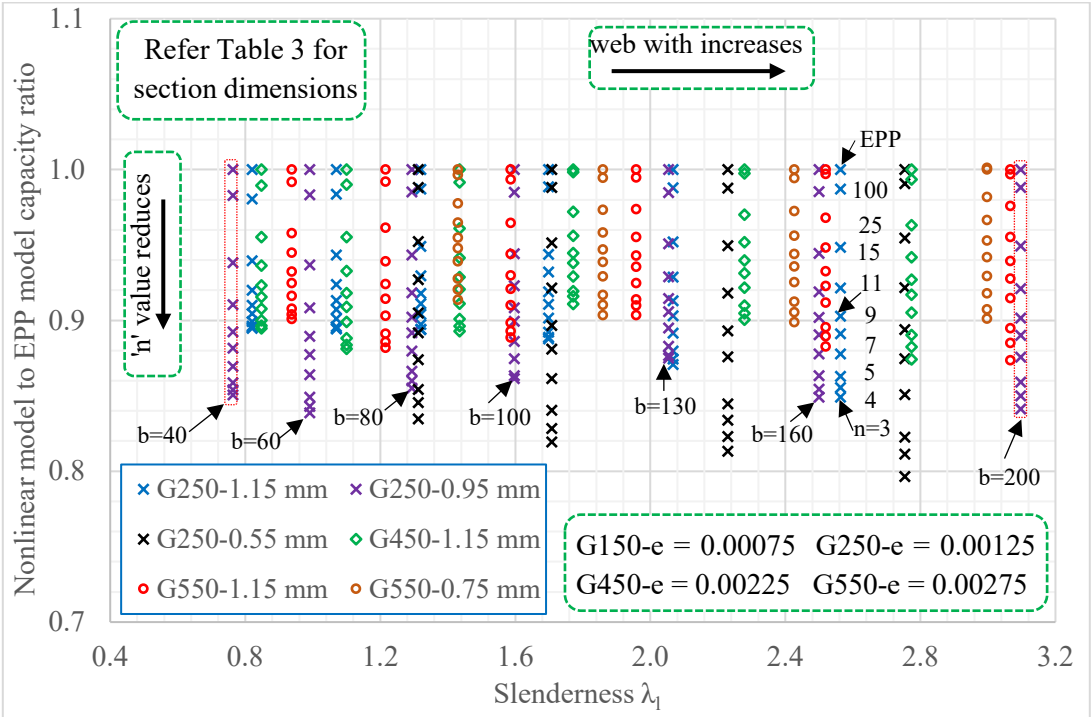

b. LCS columns with all slender elements

Fig. 7. Effects of 'n' and 'e' values on the compression capacity (local buckling).

Moreover, Fig. 7 shows that the effects of nonlinearity on the compression capacity reduce as the 'e' value increases (yield strength increases). Beskovairony et al. [10] and Rasmussen and Rondal [20, 21] observed the same effects for stainless steel and aluminium plates and columns.

The same behaviour was observed by Rokilan and Mahendran [8] for global buckling, who showed that the global buckling capacity curves of CFS columns with EPP stress-strain characteristics do not change significantly with varying 'e' values. However, Fig. 8 shows that the local buckling capacity curves change with varying 'e' values and the variation increases as the nonlinearity rises (EPP to n=3) (Fig. 9). Figs. 8 and 9 are based on the ultimate capacities of 1.15 mm thick LCS sections with one slender element (web). Similar behaviour is observed for LCS columns with all slender elements.

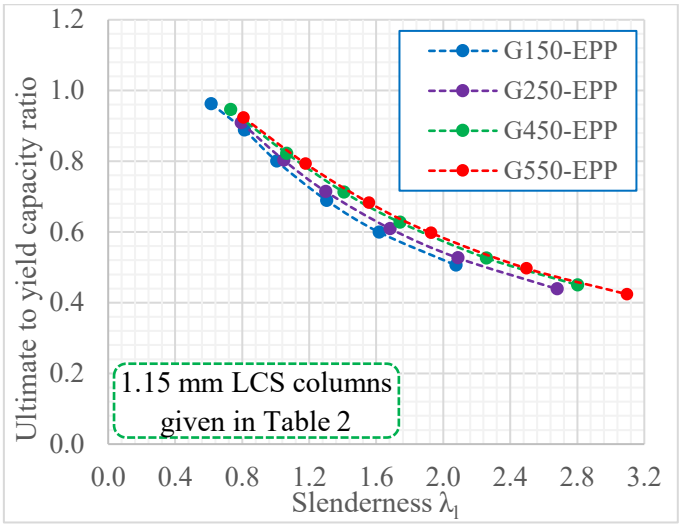

Fig. 8. Local buckling capacity curves of LCS columns with EPP stress-strain characteristics.

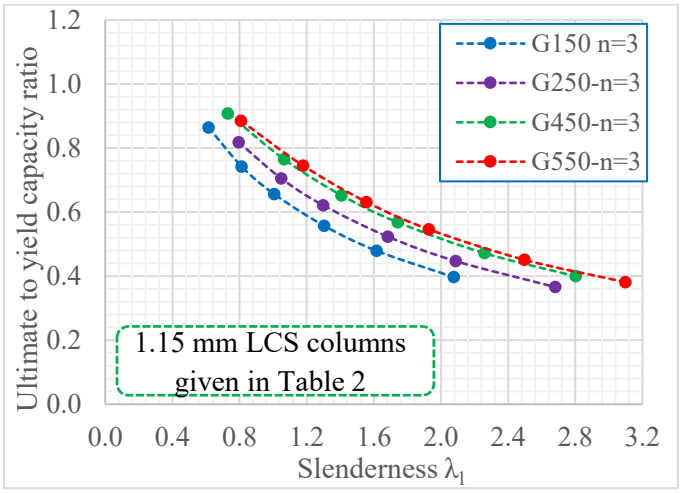

Fig. 9. Local buckling capacity curves of LCS columns with a high level of nonlinearity (n = 3).

3.2. Effects of strain hardening between yield and ultimate strengths

Rokilan and Mahendran [8] showed that the effects of strain hardening on the global buckling capacities of CFS columns are small and the effects reduce with increasing member

slenderness. However, the effect of strain hardening on the local buckling capacities of CFS columns needs to be investigated due to the difference between global and local buckling behaviour. The local buckling capacity of CFS column can be enhanced by strain hardening in two different ways: post-buckling capacity enhancement of locally buckled elements (slender elements); yield capacity enhancement of non-slender elements. Thus, G250-1.15 mm and G550-1.15 mm LCS with one slender element (web) (Table 2) and G550-1.15 mm LCS with all slender elements (Table 3) were analysed, and the resulting local buckling capacity curves are shown in Figs. 10 and 11.

It is evident from Fig. 10 that the local buckling capacity of CFS columns increases as the f_u/f_y ratio increases. However, the effect of strain hardening on local buckling capacity reduces with increasing section slenderness (λ_l) and reducing nonlinearity (n=3 to 9) (Fig. 10). On the other hand, LCS columns with all slender elements do not exhibit a considerable increment in their ultimate capacity with increasing f_u/f_y ratio. Also, the increment significantly reduces as the nonlinearity reduces (n=3 to 9) (Fig. 11). Strain hardening enhances the yield capacity of non-slender elements (flange and lip) and post-buckling capacity of slender web elements of former type LCS columns (Fig. 10) while it only influences the post-buckling capacity of latter type LCS columns (Fig. 11) as all elements are subject to local buckling. This is the reason for the different behaviour between these two types of LCS columns.

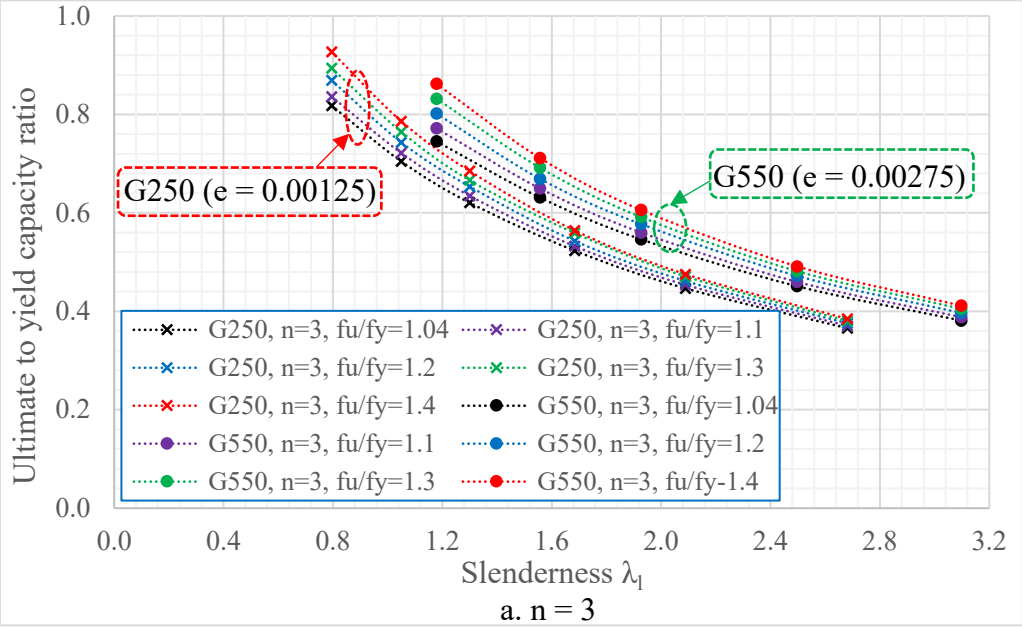

a. n = 3

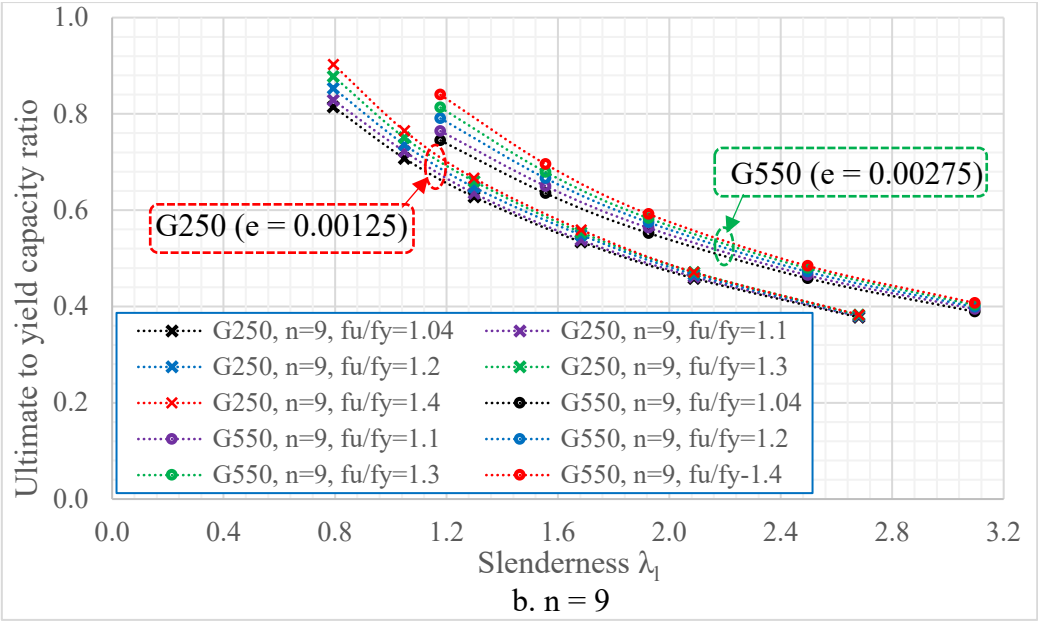

Fig. 10. Effects of strain hardening for LCS columns with one slender element (web).

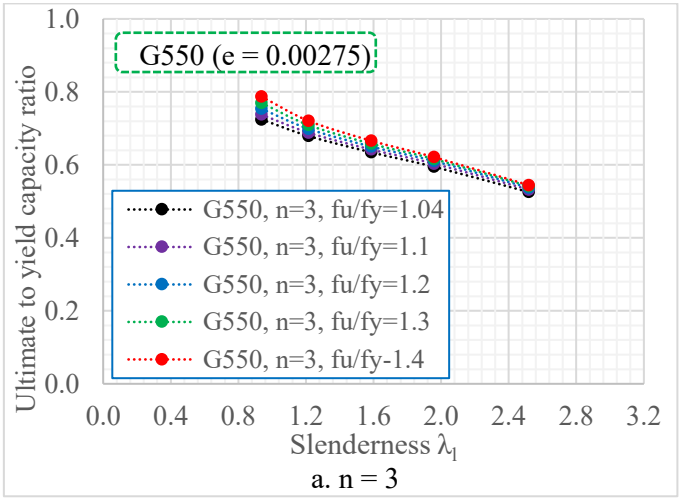

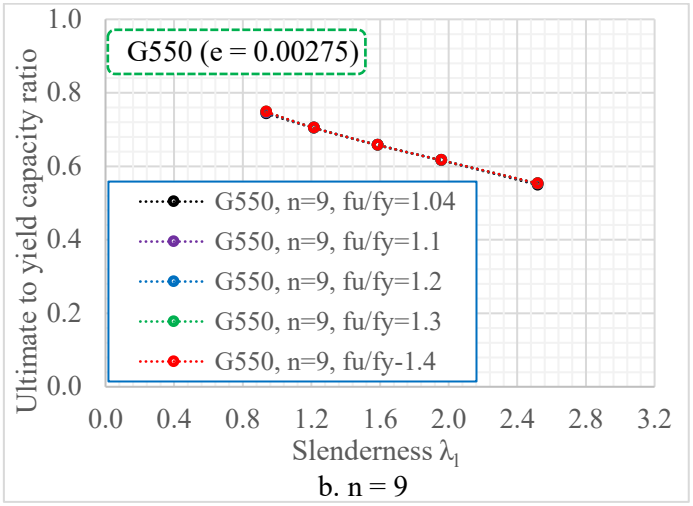

Fig. 11. Effects of strain hardening for LCS columns with all slender elements.

Stainless steel has significant strain hardening and several studies have been conducted [22, 23] to investigate the enhancement of section (yield or local) capacity of stainless steel columns due to strain hardening, which led to the proposal of continuous strength method (CSM). However, the CSM captures the enhanced capacity only for stainless steel columns with section slenderness less than 0.68. Rectangular hollow section and LCS columns with section slenderness higher than 0.68 can have non-slender elements, which can exhibit capacity enhancement due to strain hardening. However, CSM does not predict the enhanced capacity of those columns. Although CSM predicts the enhanced capacity of stainless steel columns with section slenderness less than 0.68, the CSM equations were developed using many material related factors (Fig. 12). One material related factor (C_2) is used along with yield strength, ultimate stress and yield and ultimate strains to determine the second slope of the CSM bilinear stress-strain model (linear hardening model) converted from the original nonlinear stress-strain model. Another material related factor (C1) is used to avoid unsafe prediction from the converted CSM bilinear stress-strain model [22]. These CSM approaches show that the capacity enhancement due to strain hardening cannot be captured by only using 'n' and 'e' factors and ultimate stress and strain. Moreover, CSM does not recognise the effects of nonlinearity between proportional limit stress and yield strength. Thus, development and application of CSM based design equations to incorporate the capacity enhancement due to strain hardening is quite complex.

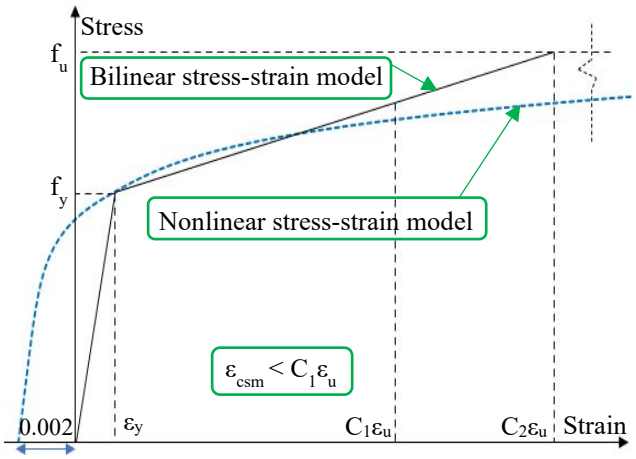

Fig. 12. Bilinear stress-strain model used in CSM.

On the other hand, the Eurocode 3 Part 1-2 [24] approach of using the stress at 2% total strain as the yield strength of non-slender sections can be used since high strains can be allowed under fire conditions. As per Eurocode 3 Part 1-2 [24] no element can be slender in a non-slender

section. Thus, element slenderness needs to be checked against the stress at 2% total strain instead of yield strength. However, commonly used CFS lipped channel sections have at least one slender element due to their small thicknesses. Therefore, this paper conservatively neglects the effects of strain hardening on the local buckling capacity of CFS columns at elevated temperatures.

4. Evaluation of current design methods

This section focuses on a review of current elevated temperature design equations of CFS sections and compares the ultimate capacities obtained from FE analysis (FEA) and current AS/NZS 4600 [9] equations. AS/NZS 4600 recommends the use of ambient temperature local buckling capacity equations with elevated temperature mechanical properties. However, this design method cannot be used if the proportional limit stress to yield strength ratio is less than 0.75. Similar to AISI S100 [25], ambient temperature local buckling capacities of CFS columns can be determined using either the Direct Strength Method (DSM) or the Effective Width Method (EWM) in AS/NZS 4600. Thus, the modified design method based on AS/NZS 4600 can also be used for AISI S100, which does not give any elevated temperature design equations. In this section, the AS/NZS 4600 design capacities were obtained without considering the limit of 0.75 for the proportional limit stress to yield strength ratio.

Eurocode 3 Part 1-2 [24] recommends a critical temperature of 350 ℃ for class 4 sections. Yield strength (0.2% proof stress) reduction factor of class 4 section is 0.72 at 350 ℃ as per Eurocode 3 Part 1-2, which uses the same mechanical property reduction factors for hot-rolled and cold-formed steels. However, the critical temperature of 350 ℃ is questionable for low strength CFS sections as its yield strength reduction factor is 0.56 as per AS/NZS 4600 [9], ie 77% less than 0.72 at 350 ℃. Eurocode 3 Part 1-2 also recommends the use of ambient temperature design capacity equations with elevated temperature yield strength (relevant to class 4 sections) and ambient temperature effective cross-section area. It modifies the ambient temperature yield strength dependent parameter ($\varepsilon = \sqrt{235/f_y}$) by a factor of 0.85 for the cross-section classification. Earlier versions of Eurocode 3 Part 1-2 used $\sqrt{K_{ET}/K_{yT}}$ instead of 0.85, where K_{ET} is the ratio of elevated temperature Young's modulus to ambient temperature Young's modulus (E_T/E_{20}) and K_{yT} is the ratio of elevated temperature yield strength to ambient temperature yield strength ($f_{y,T}/f_{y,20}$), and then it was replaced by the average value of 0.85. However, the design standard does not consider the effects of varying yield strength

to Young's modulus ratio in the effective area calculation as the design standard recommends using the ambient temperature effective area. This approach will lead to less accurate predictions than AS/NZS 4600 elevated temperature effective width method (EWM) predictions, which uses the elevated temperature effective cross-section area. In addition, the EWM calculations of Eurocode 3 Part 1-2 are more complex than those of AS/NZS 4600 due to the iteration process. It will result in a complex method when the effects of nonlinearity are considered. Thus, this paper evaluates only the accuracy of AS/NZS 4600 EWM and DSM predictions.

4.1. Effective width method (EWM) - AS/NZS 4600

Fig. 13 compares the local buckling capacities of CFS columns acquired from the FEA based parametric study with those predicted by the EWM in AS/NZS 4600 (Eqs. 8 to 11) [9]. It shows that AS/NZS 4600 (Eqs. 8 and 9) gives unsafe predictions in many cases. The FEA to AS/NZS 4600 capacity ratio of LCS columns with one slender element (web) falls below 0.85 (Fig. 13 (a)) in many cases, especially for CFS columns with a high level of nonlinearity (lower 'n' values) and smaller 'e' value (lower yield strength). Therefore, the effects of nonlinear stress-strain characteristics of CFS columns at elevated temperatures should be included in the design equations.

For $\lambda \leq 0.673$: $b_e = b$ (8)

For $\lambda > 0.673$: $b_e = \rho b$ (9)

Where b and b_e are plate width and effective width, respectively, while effective width factor (ρ) and slenderness ratio (λ) can be determined from Eqs. 10 and 11, respectively.

$$\rho = \frac{1}{\lambda} - \frac{0.22}{\lambda^2} \leq 1.0 \quad (10)$$

$$\lambda = \sqrt{f^*/f_{cr}} \quad (11)$$

Where f^* and f_{cr} are design stress in the compression element and plate elastic buckling stress, which can be calculated from Eq. 12, respectively. In this study, f^* was taken as yield strength (f_y) since global buckling is not present.

$$f_{cr} = \frac{k\pi^2 E}{12\,(1-\nu^2)} \left(\frac{t}{b}\right)^2 \quad (12)$$

Where k, E, v, t and b are plate buckling coefficient, Young's modulus, Poisson's ratio, plate thickness and width, respectively.

The FEA to AS/NZS 4600 capacity ratio of LCS columns with all slender elements falls between 0.87 and 1.18 while that of LCS columns with one slender element (web) falls between 0.76 and 1.06. Moreover, Australian open CFS exhibit smaller values for both 'n' and 'e' factors only at some temperatures (Table 4). Thus, an extended investigation was conducted using the measured stress-strain curves of G250 and G550 Australian open CFS sections at elevated temperatures (Fig. 14). 1.15 mm G250 and G550 LCS columns with one slender element (web) were selected here since AS/NZS 4600 EWM gives lower FEA to AS/NZS 4600 capacity ratios for LCS columns with one slender element (web) (Fig. 13 (a)) than for those with all slender elements (Fig. 13 (b)). Also, the effects of 'n' and 'e' factors do not significantly vary with the cross-section dimensions at given slenderness (λ_l).

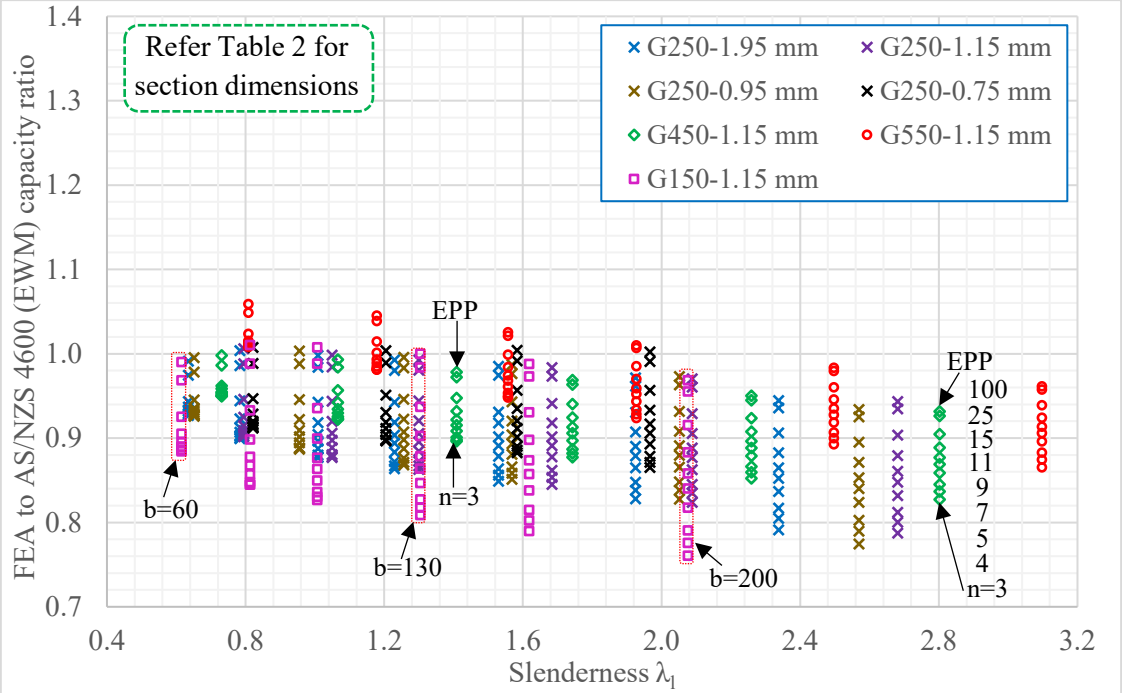

a. LCS columns with one slender element (web)

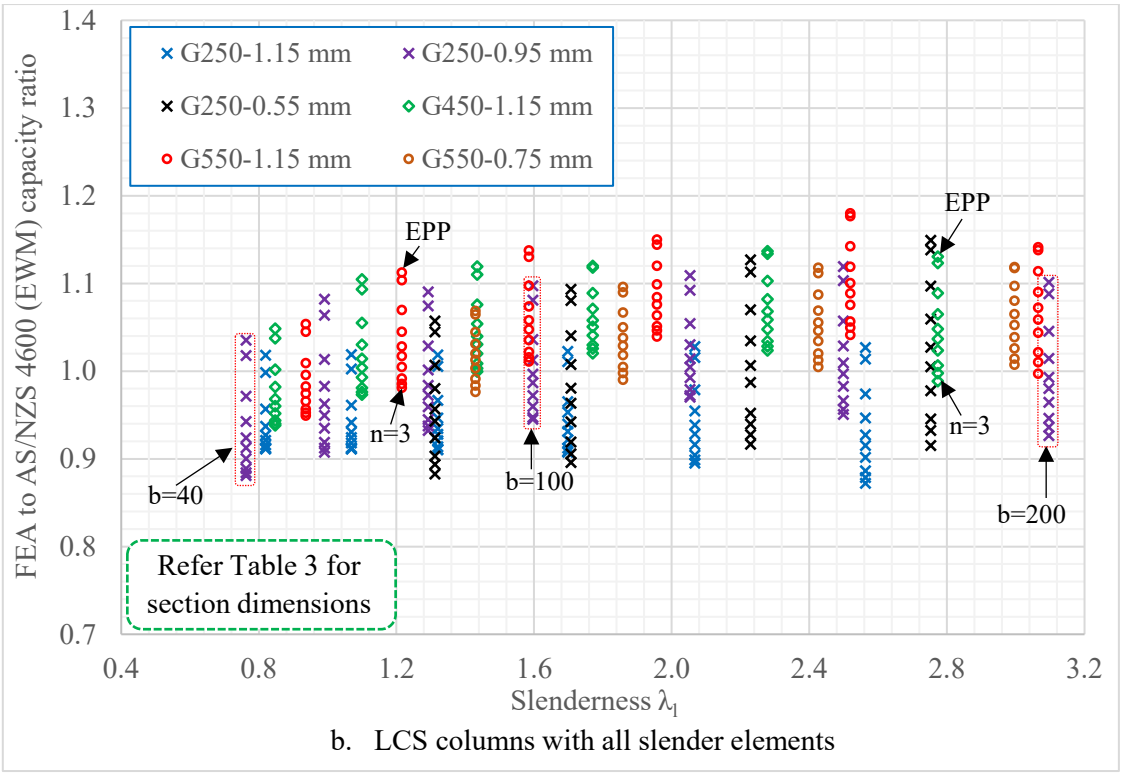

Fig. 13. Comparison of FEA and AS/NZS 4600 EWM local buckling capacities of CFS columns with idealised stress-strain curves.

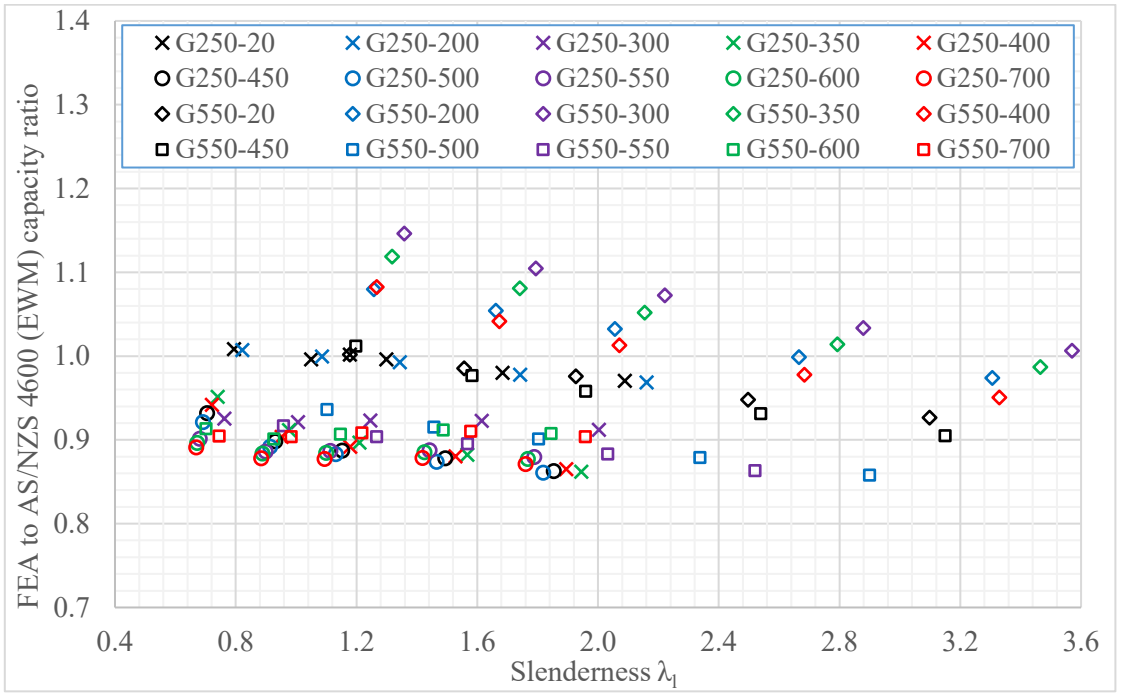

Fig. 14. Comparison of FEA and AS/NZS 4600 EWM local buckling capacities of CFS columns with measured elevated temperature stress-strain curves.

The FEA to AS/NZS 4600 capacity ratios in Fig. 14 are in the range of 0.85 to 1.15 and the corresponding capacity reduction factor is 0.85 with COV of 0.07 as shown in Table 5. Thus, it is possible to conclude that the effects of elevated temperature nonlinear stress-strain characteristics are not significantly affecting the design capacity prediction. The ultimate compression capacity of Australian open CFS sections subject to local buckling can be therefore determined using the ambient temperature AS/NZS 4600 EWM and the elevated temperature mechanical properties. However, modified design equations proposed in Section 5.1 should be used for CFS sections made of other steels (not Australian grade steels).

4.2. Direct strength method (DSM) - AS/NZS 4600

Fig. 15 compares the local buckling capacities of LCS columns obtained from FEA with those predicted by the DSM in AS/NZS 4600 (Eqs. 13 and 14) [9]. The FEA to DSM capacity ratios show more deviations (0.76 to 1.12 and 0.72 to 1.35 in Fig. 15) than the FEA to EWM capacity ratios (0.76 to 1.06 and 0.87 to 1.18 in Fig. 13) as DSM is based on section slenderness (λ_l) whereas EWM is based on element slenderness (λ). Kumar and Kalyanaraman [26] highlighted the deficiencies in the use of DSM for CFS columns at ambient temperature and proposed a modified DSM by incorporating flange width to web width ratio. Also, they showed that DSM gives unsafe predictions for lower values of λ_l, and changed the limiting λ_l of 0.776 to 0.60. The section capacity is equal to the yield capacity for cross-sections with λ_l values less than 0.776 as per the DSM (Eq. 13). Deficiencies in using 0.776 as the limiting value can be seen from FEA to DSM capacity ratios of CFS columns with EPP stress-strain curves in Fig. 15 (a). The reason for the lower FEA to DSM capacity ratios observed for G250-0.55 mm and G550-0.75 mm columns (Fig. 15 (b)) is not using the flange width to web width ratio in the DSM equations. The unsafe prediction given by the ambient temperature DSM is further increased by the effects of elevated temperature nonlinear stress-strain characteristics of CFS. Therefore the effects of nonlinear stress-strain characteristics of CFS columns at elevated temperatures should be incorporated into the DSM equations of AS/NZS 4600 since they give unsafe predictions in many cases (Fig. 15).

$$\text{For } \lambda_l \leq 0.776\text{: } N_{cl} = N_{ce} \tag{13}$$

$$\text{For } \lambda_l \leq 0.776\text{: } N_{cl} = N_{ce}\left[1 - 0.15\left(\frac{N_{ol}}{N_{ce}}\right)^{0.4}\right]\left(\frac{N_{ol}}{N_{ce}}\right)^{0.4} \tag{14}$$

$$\lambda_l = \sqrt{N_{ce}/N_{ol}} \tag{15}$$

Where N_{ce} and N_{ol} are the global buckling and elastic local buckling capacities while non-dimensional slenderness (λ_l) can be determined from Eq. 15. In this study, N_{ce} was taken as the yield capacity (N_y) since there is no capacity reduction due to global buckling and N_{ol} was taken from FEA.

The ultimate compression capacities obtained using the measured elevated temperature stress-strain curves of G250 and G550 Australian open CFS sections (Table 4) were also compared with DSM in Fig. 16. It shows that the FEA to DSM capacity ratios of low strength steel (G250) columns in the temperature range of 300 to 700 °C and high strength steel (G550) columns in the temperature range of 550 to 700 °C are well below 0.9. Moreover, the unsafe predictions of DSM are high for LCS columns with all slender elements than for those with one slender element (web) when the section slenderness (λ_l) is small (Fig. 15). Generally, web and flanges of commercial lipped channel sections are slender. Although the effects of nonlinear stress-strain characteristics could be ignored when using the EWM for Australian open CFS sections, such effects cannot be neglected when using the DSM due to the deficiencies of ambient temperature DSM equations as discussed previously. However, a simplified design method is proposed in Section 5.2 for Australian open CFS sections in addition to the modified DSM proposed for any open CFS sections.

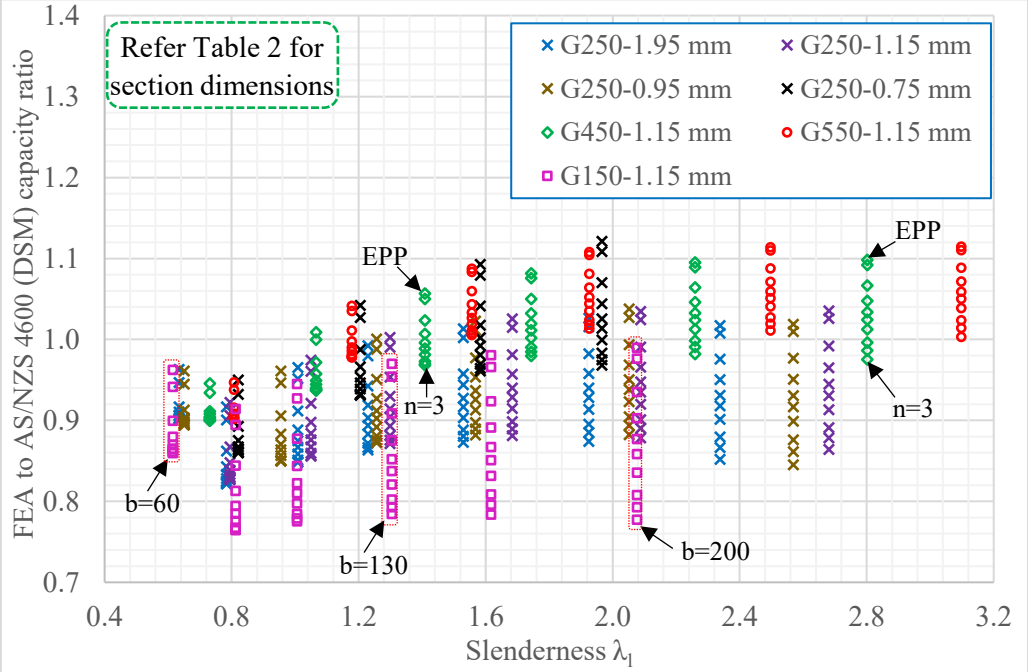

a. LCS columns with one slender element (web)

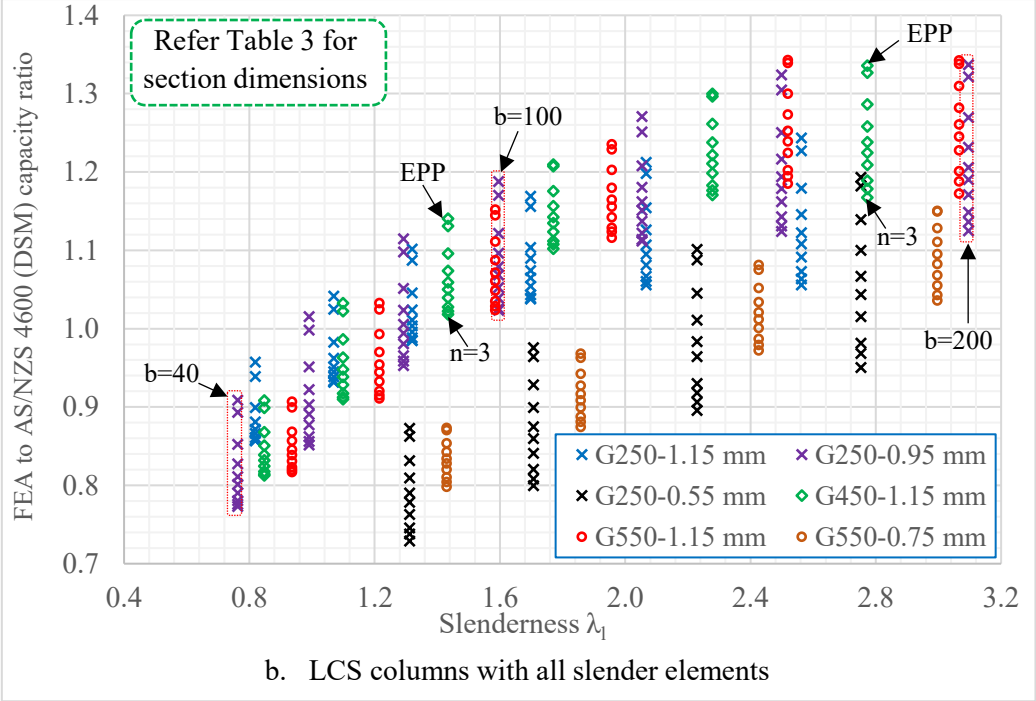

b. LCS columns with all slender elements

Fig. 15. Comparison of FEA and AS/NZS 4600 DSM local buckling capacities of CFS columns with idealised stress-strain curves.

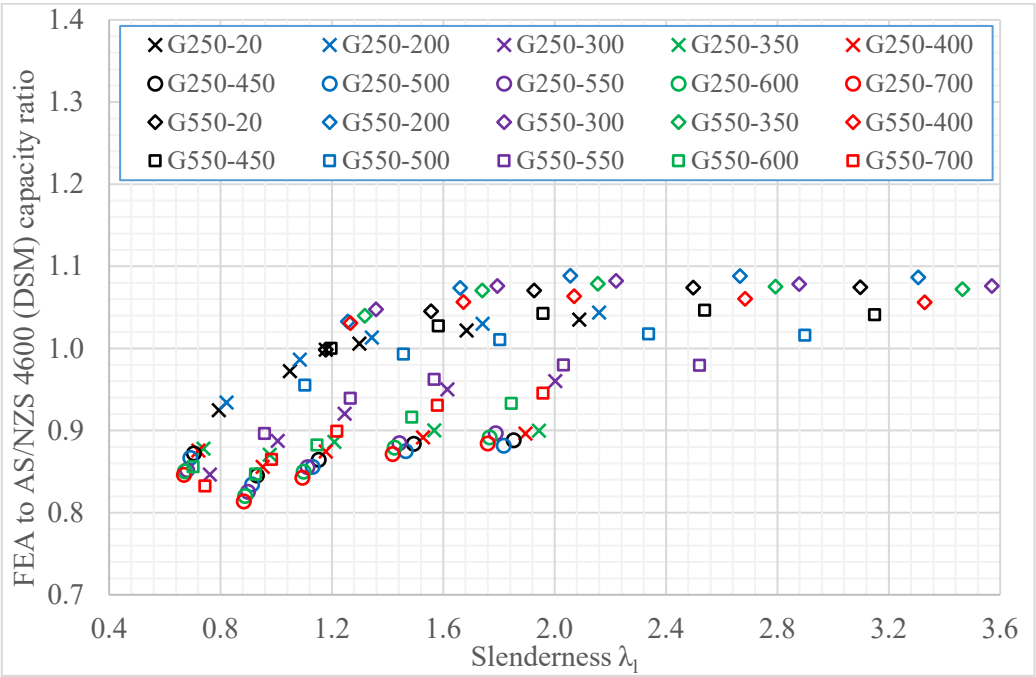

Fig. 16. Comparison of FEA and AS/NZS 4600 DSM local buckling capacities of CFS columns with measured elevated temperature stress-strain curves.

5. Modified design methods

AS/NZS 4673 [27] does not consider the effects of nonlinearity and varying yield strength to Young's modulus ratio of stainless steel on their section capacities although it considers these effects on the global buckling capacities. Rasmussen et al. [28] showed that although the effects of gradual yielding reduce the section capacity of stainless steel columns, it is compensated by the increased yield strength at the corners of cold-formed stainless steel sections. This may be the reason why AS/NZS 4673 does not consider the effects of nonlinearity and varying yield strength to Young's modulus ratio. Eurocode 3 Part 1-4 [29] uses three different modified Winter [30] curves based on the type of production (cold-formed or welded) and element type (internal or outstanding). However, it is unclear whether the effects of nonlinearity are included in these curves while Rasmussen et al. [28] reports that all three curves can be represented by a single curve, which is about 10% below the Winter [30] curve.

This paper has shown that the effects of nonlinearity and varying yield strength to Young's modulus ratio on the local buckling capacities are less than those on the global buckling capacities [8]. Also, Section 4 has shown that the effects of nonlinear stress-strain characteristics can be neglected if the EWM is used to determine the ultimate compression capacities of commercially used Australian open CFS columns subject to local buckling. However, Fig. 13 shows that the current AS/NZS 4600 EWM gives unsafe predictions for certain 'n' and 'e' values, which may represent many other CFS sections that are not made of Australian CFS. On the other hand, Figs. 15 and 16 show that the current DSM equations also give unsafe predictions for certain 'e' values and section slenderness (λ_l). Thus, modified design methods are proposed for AS/NZS 4600 EWM and DSM by incorporating the effects of nonlinearity (n) and varying yield strength to Young's modulus ratio (e). Effects of strain hardening on the local buckling capacity are not included as discussed in Section 3.2.

5.1. Modified EWM for AS/NZS 4600

Bezkorovainy et al. [10] proposed a modified Winter [30] equation in the form of Eq. 16 to determine the local buckling capacities of metal plates by incorporating the effects of nonlinearity (n) and varying yield strength to Young's modulus ratio (e). The EWM in AS/NZS 4600 [9] is also based on the Winter [30] equation. Hence, the same design method is proposed to determine the elevated temperature local buckling capacities of CFS columns. The effects of strain hardening are not considered in the modified design equations as discussed in Section

3.2. Although Bezkorovainy et al. [10] developed the equations based on the ultimate compression capacities of plates that include the effects of strain hardening, the design equations predict the ultimate compression capacities of CFS columns that do not include the effects of strain hardening. This indicates that the capacity enhancement due to strain hardening is significantly less in their study compared to the capacity reduction due to 'n' and 'e' factors. Following Bezkorovainy et al.'s [10] method, the effective width factor (ρ) is modified by using two coefficients α and β (Eq. 16), which depend on the elevated temperature 'n' and 'e' values of CFS sections. Eqs. 16 to 20 were used to predict the local buckling capacities of CFS columns, which are compared with FEA capacities in Fig. 17. It shows that the unsafe predictions observed in Fig. 13 are significantly reduced by the modified design equations.

$$\rho = \frac{\alpha}{\lambda} - \frac{\beta}{\lambda^2} \leq 1.0 \tag{16}$$

where, α and β can be calculated using Eqs. 17 to 20, respectively, if the 'n' value is less than 100. Otherwise, they are 1 and 0.22, respectively. Also, λ is element slenderness defined as $\sqrt{f_y/f_{cr}}$, and f_y and f_{cr} are yield and plate elastic buckling stress, respectively.

For $3 \leq n \leq 10$:

$$\alpha = 0.92 + 0.07 \tanh\left(\frac{n-3}{2.1}\right) - (0.026 \exp[-0.55(n-3)] + 0.019)(6 - 2000e) \leq 1.0 \tag{17}$$

For $10 < n < 100$: $$\alpha = \alpha_{10} + (1 - \alpha_{10})\left(\frac{n-10}{90}\right) \leq 1.0 \tag{18}$$

For $3 \leq n \leq 10$:

$$\beta = 0.18 + 0.045 \tanh\left(\frac{n-3}{2.5}\right) - (0.01 \exp[-1.6(n-3)] + 0.005)(6 - 2000e) \leq 0.22 \tag{19}$$

For $10 < n < 100$: $$\beta = \beta_{10} + (0.22 - \beta_{10})\left(\frac{n-10}{90}\right) \leq 0.22 \tag{20}$$

where, the values of 'n' and 'e' are based on the elevated temperature stress-strain characteristics of CFS used. Also, α_{10} and β_{10} are values of α and β calculated for the 'n' value of 10, respectively.

Rasmussen et al. [28] introduced a modified limiting value λ_y in terms of α and β, which can be determined from Eq. 21, instead of the limiting value of 0.673. However, $(\alpha^2 - 4\beta)$ in Eq. 21 can be less than zero in some cases based on the 'n' and 'e' values, which makes λ_y a complex number. Thus, the original limiting value of 0.673 in Eqs. 8 and 9 was not changed in

this modified method. Although the local buckling capacity of CFS columns is reduced at slenderness less than 0.673 due to the nonlinearity between proportional limit stress and yield strength, it is increased by strain hardening at that slenderness. Figs. 10 and 11 show that the effect of strain hardening increases as the slenderness reduces. Thus, it is not necessary to reduce the existing limiting slenderness value of 0.673.

$$\lambda_y = \left(\alpha + \sqrt{\alpha^2 - 4\beta}\right)/2 \tag{21}$$

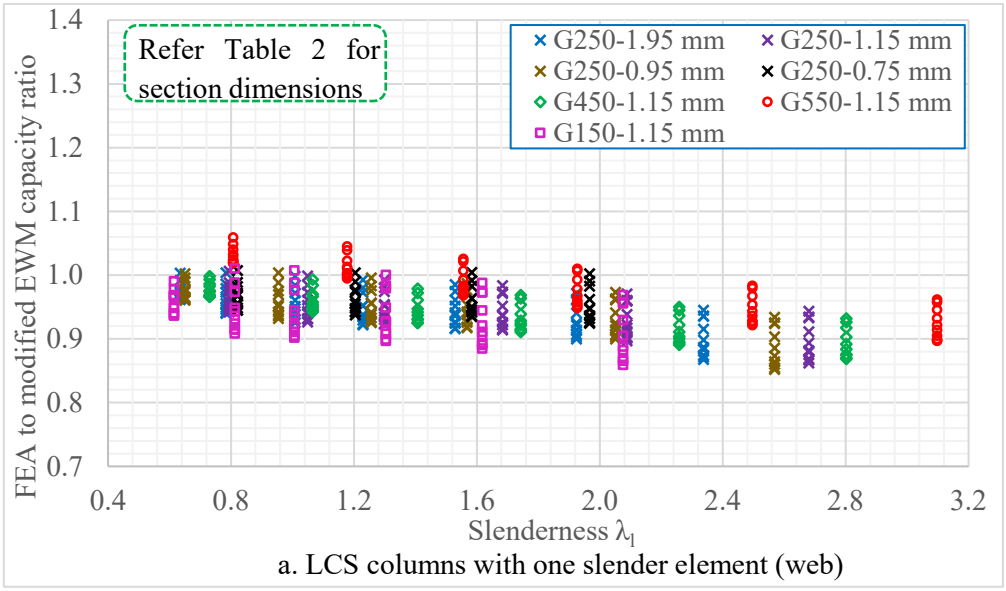

a. LCS columns with one slender element (web)

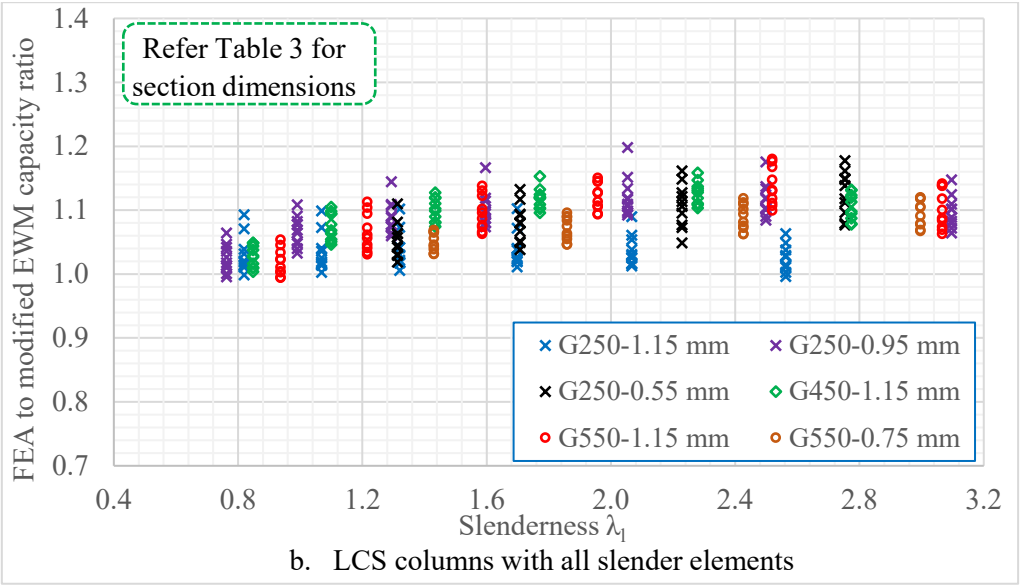

b. LCS columns with all slender elements

Fig. 17. Comparison of FEA and modified EWM local buckling capacities of CFS columns with idealised stress-strain curves.

5.2. Modified and simplified DSM for AS/NZS 4600

Although EWM gives more accurate predictions, CFS designers tend to use DSM due to its easier application. Thus, the current DSM based equations (Eqs. 13 and 14) are modified (Eqs. 22 and 23) to incorporate the effects of nonlinearity (n) and yield strength to Young's modulus ratio (e). Since the current ambient temperature DSM equations give overconservative or unsafe predictions even for CFS columns with elastic perfect plastic stress-strain models as shown in Fig. 15(b), they need to be modified through further parametric studies of different types of open CFS sections. However, the same DSM equations (Eqs. 22 and 23) are proposed here with a modified slenderness $\lambda_{l,m}$ to include the effects of nonlinear elevated temperature stress-strain characteristics. Comparison of capacities in Figs. 18 and 19 show that the unsafe predictions of current DSM equations (Figs. 15 and 16) due to the presence of nonlinearity and yield strength to Young's modulus ratio are reduced by the modified DSM equations.

For $\lambda_{l,m} \leq 0.776$: $N_{cl} = N_y$ (22)

For $\lambda_{l,m} \leq 0.776$: $N_{cl} = N_y \left[1 - 0.15 \left(\frac{N_{ol}}{N_y}\right)_m^{0.4}\right] \left(\frac{N_{ol}}{N_y}\right)_m^{0.4}$ (23)

where, $\left(\frac{N_{ol}}{N_y}\right)_m = \left(\frac{1}{\lambda_{l,m}}\right)^2$ and the modified section slenderness $\lambda_{l,m}$ can be calculated from Eq. (24) if the 'n' value is less than 100. Otherwise, it is equal to λ_l.

$$\lambda_{l,m} = \lambda_l + [0.33 - 0.09 \ln(n)] [0.0027/e]^{0.8} [1 - 1/(n\lambda_l)^{0.8}] \geq \lambda_l \quad (24)$$

where, λ_l is section slenderness and the values of 'n' and 'e' are based on the elevated temperature stress-strain characteristics of CFS used. Although Rokilan and Mahendran [8] ignored the effects of nonlinear stress-strain characteristics on the global buckling capacity of CFS columns with 'n' values greater than 15, the limiting value is taken as 100 for local buckling. Fig. 15 shows that the current DSM equations give unsafe predictions even for CFS columns with EPP stress-strain models at lower slenderness. On the other hand, reduced 'e' values observed at elevated temperatures reduce the elevated temperature slenderness of CFS columns than those at ambient temperature. Moreover, 'e' values significantly affect the local buckling capacities of CFS columns than their global buckling capacities when the effects are combined with the those of 'n' values. Thus, the limiting 'n' value is taken as 100.

Section 4.2 showed that the FEA to DSM capacity ratios of low strength steel (G250) in the temperature range of 300 to 700 ℃ and high strength steel (G550) in the temperature range of 550 to 700 ℃ are well below 0.9 (Fig. 16). Thus, a reduction factor of 0.9 is proposed for Australian high and low strength open CFS sections exposed to those temperature ranges. When this factor is used, Fig. 20 shows that FEA to DSM capacity ratios are above 0.9 while Table 5 shows that the capacity reduction factor and COV are 0.91 and 0.05, respectively, demonstrating further improvements. Also, this paper recommends the use of EWM instead of DSM if the flange width to web width ratio is less than 1.5.

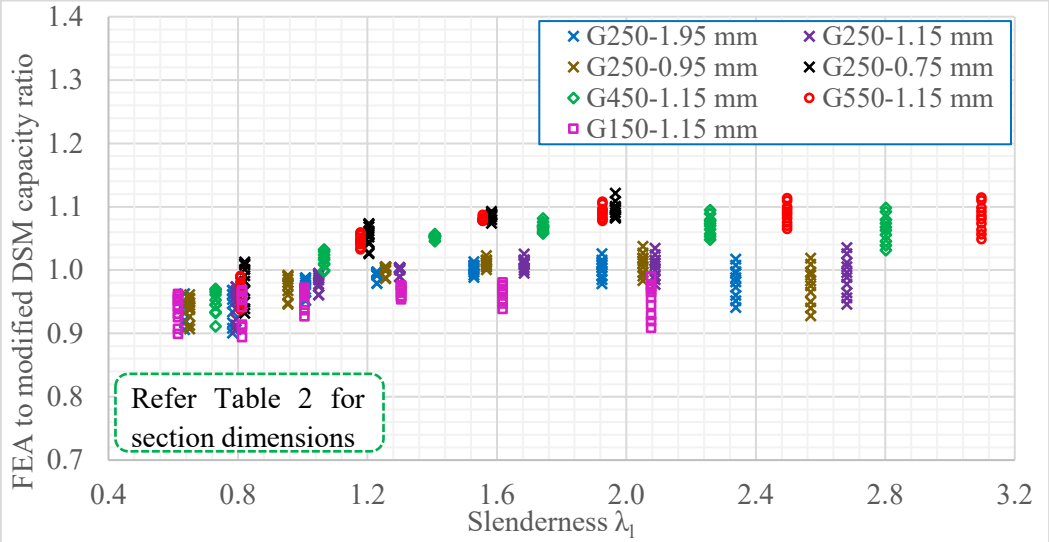

a. LCS columns with one slender element (web)

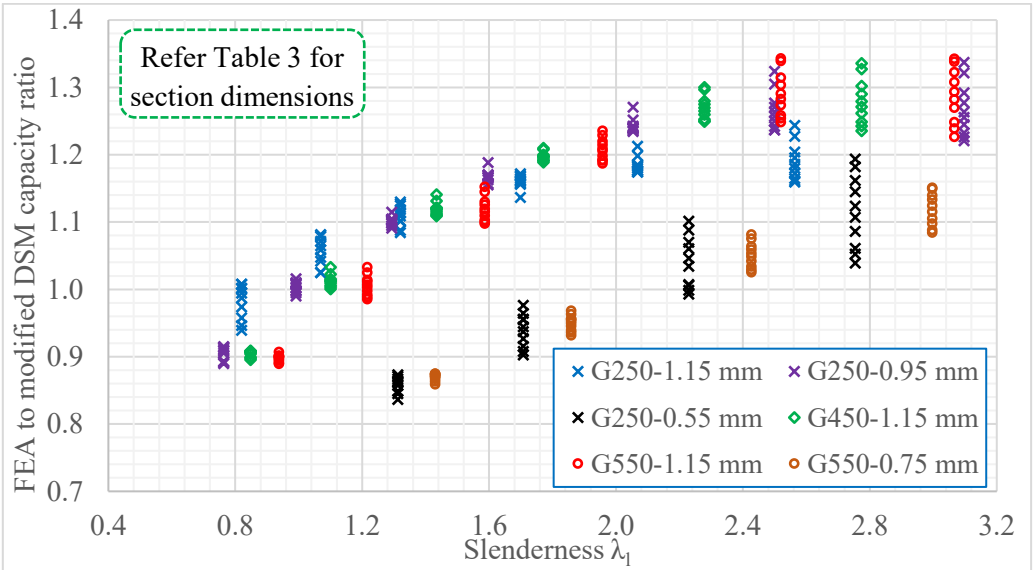

b. LCS columns with all slender elements

Fig. 18. Comparison of FEA and modified DSM local buckling capacities of CFS columns with idealised stress-strain curves.

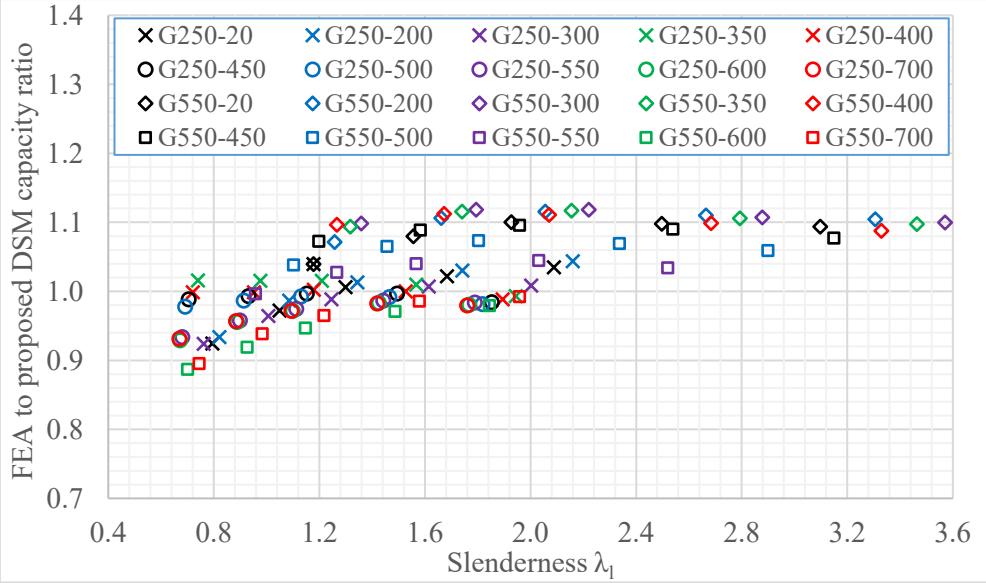

Fig. 19. Comparison of FEA and modified DSM local buckling capacities of CFS columns with measured elevated temperature stress-strain curves.

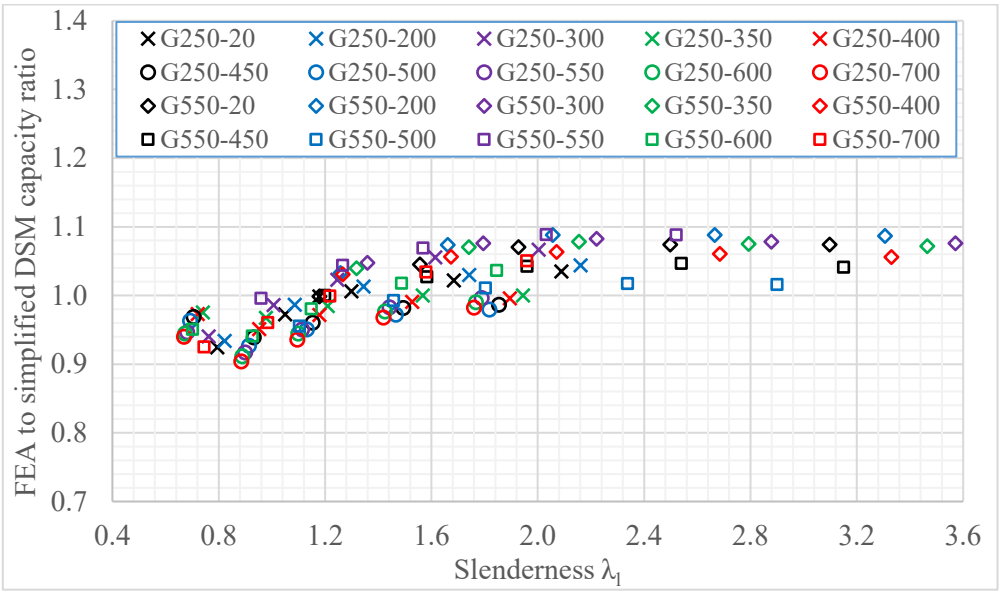

Fig. 20. Comparison of FEA and simplified DSM local buckling capacities of CFS columns with measured elevated temperature stress-strain curves.

5.3. Capacity reduction factor (ϕ)

Suitable capacity reduction factors were computed for the current and modified design methods using the statistical model (Eq. 25) given in AISI S100 [25]. In Eq. 25, M_m and V_m are the mean and COV of the material factor = 1.1 and 0.1, F_m and V_f are the mean and COV of the fabrication factor = 1.0 and 0.05, Vq is the COV of the load factor = 0.21 and β_0 is the target

reliability index of 2.5. In this study, since the number of tests n is 410, 330 and 100 for LCS with one slender element (web), LCS with all slender elements and LCS used with the measured elevated temperature stress-strain curves, respectively, the correction factor $C_p = \frac{m\,(1+1/n)}{m-2}$ is determined as 1.007, 1.009 and 1.031. Table 5 presents the mean and COV of the FEA to design method capacity ratio and the capacity reduction factors (ϕ).

$$\phi = 1.52\, M_m F_m P_m e^{-\beta_0 \sqrt{V_m^2 + V_f^2 + C_p V_p^2 + V_q^2}} \quad (25)$$

Table 5. Capacity reduction factors for AS/NZS 4600 design methods.

Design method	Used stress-strain curves	Section type	Mean (P_m)	COV (V_p)	ϕ
Current EWM	Idealised	LCS – slender web	0.92	0.06	0.83*
		LCS – all slender elements	1.01	0.07	0.91
		Both types LCS	0.96	0.08	0.85
	Measured	LCS – slender web	0.94	0.07	0.85
Current DSM	Idealised	LCS – slender web	0.94	0.08	0.84
		LCS – all slender elements	1.04	0.14	0.87
		Both types LCS	0.98	0.13	0.84
	Measured	LCS – slender web	0.95	0.09	0.84
Modified EWM	Idealised	LCS – slender web	0.95	0.04	0.86*
		LCS – all slender elements	1.08	0.04	0.97*
		Both types LCS	1.01	0.08	0.90
Modified DSM	Idealised	LCS – slender web	1.00	0.05	0.91*
		LCS – all slender elements	1.10	0.12	0.94
		Both types LCS	1.05	0.10	0.91
	Measured	LCS – slender web	1.02	0.06	0.92*
Simplified DSM	Measured	LCS – slender web	1.01	0.05	0.91*
ϕ* - obtained using the minimum COV of 0.065 as per AISI S100					

The mean values are less than 1.0 with higher COVs for the current EWM and DSM, which often lead to ϕ factors less than 0.85, which is the current ϕ factor for compression members. The modified design methods proposed in this paper improve this situation by eliminating the

unsafe predictions in most cases, thus increasing the mean values with reduced COVs, and thus to ϕ factors greater than 0.85.

6. Conclusions

In this study, a detailed numerical investigation was conducted to investigate the effects of the nonlinear stress-strain characteristics of CFS at elevated temperatures on the local buckling capacities of CFS columns. The nonlinear stress-strain characteristics were broadly categorised into three different areas, namely, nonlinearity between proportional limit stress and yield strength (n), strain hardening between yield and ultimate strengths and the yield strength to Young's modulus ratio (e). The main findings of this study are as follows.

1. It was observed that all three parameters (n, e and strain hardening) affect the elevated temperature local buckling capacities of CFS columns. Their effects are interrelated and depend on element or section slenderness. The current EWM and DSM design equations in AS/NZS 4600 for CFS columns subject to local buckling provided both conservative and unsafe capacity predictions for different 'n', 'e' and slenderness values.
2. Modified design equations incorporating the effects of nonlinearity (n) and varying yield strength to Young's modulus ratios (e) were proposed based on AS/NZS 4600. Strain hardening effects were conservatively neglected to avoid complexity in the design equations as CFS columns with all slender elements do not show significant capacity enhancement.
3. This paper has recommended the use of AS/NZS 4600 EWM without any modification for commonly used Australian open CFS sections.
4. This paper has recommended either the use of the current DSM with an additional capacity reduction factor of 0.9 in the temperature range of 300 to 700 °C and 550 to 700 °C for low and high strength CFS sections, respectively, or the modified DSM for Australian open CFS sections.

Acknowledgements

The authors wish to thank Queensland University of Technology and Australian Research Council (Grant Number LP170100951) for providing financial support including a PhD scholarship and necessary facilities to conduct this research.

References

[1] C. H. Pham, G. J. Hancock, Shear tests and design of cold-formed steel channels with central square holes, Thin-Walled Structures, 149 (2020) 106650.

[2] A. D. Ariyanayagam, M. Mahendran, Fire performance of load bearing LSF wall systems made of low strength steel studs, Thin-Walled Structures 130 (2018) 487-504.

[3] A. D. Ariyanayagam, M. Mahendran, Experimental study of non-load bearing light gauge steel framed walls in fire, Journal of Constructional Steel Research 145 (2018) 529-551.

[4] E. Steau, M. Mahendran, Fire Resistance Behaviour of LSF Floor-Ceiling Configurations, Thin-Walled Structures 156 (2020) 106860.

[5] J. Chen, B. Young, Cold-formed steel lipped channel columns at elevated temperatures, Engineering Structures 29 (10) (2007) 2445-2456.

[6] S. Gunalan, Y. Bandula Heva and M. Mahendran, Local buckling studies of cold-formed steel compression members at elevated temperatures, Journal of Constructional Steel Research 108 (2015) 31-45.

[7] M. Rokilan, M. Mahendran, Elevated temperature mechanical properties of cold-rolled steel sheets and cold-formed steel sections, Journal of Constructional Steel Research 167 (2020) 105851.

[8] M. Rokilan, M. Mahendran, Effects of nonlinear elevated temperature stress-strain characteristics on the global buckling capacities of cold-formed steel columns, Thin-Walled Structures, 160 (2021)107352.

[9] Standards Australia, AS/NZS 4600, Cold-formed Steel Structures, Sydney, Australia, 2018.

[10] P. Bezkorovainy, T. Burns, K.J.R. Rasmussen, Strength curves for metal plates in compression, Journal of Structural Engineering 129 (11) (2003) 1433-1440.

[11] Dassault Systems Simulia Corporation, ABAQUS (Analysis User's Guide), USA, 2017.

[12] H. D. Craveiro, J. P. C. Rodrigues, L. Laı´m, Cold-formed steel columns made with open cross-sections subjected to fire, Thin-Walled Struct 85 (2014) 1–14.

[13] M. Feng, Y. C. Wang, J. M. Davies, Structural behaviour of cold-formed thin-walled short steel channel columns at elevated temperatures. Part 1: experiments, Thin-Walled Struct 41(2003) 543–570.

[14] H. D. Craveiro, J. P. C. Rodrigues, L. Laı´m, Experimental analysis of built-up closed cold-formed steel columns with restrained thermal elongation under fire conditions, Thin-Walled Struct 107 (2016) 564–579.

[15] J. H. Lee, Local buckling behaviour and design of cold-formed steel compression members at elevated temperatures PhD. Thesis, Queensland University of Technology, Australia (2004).

[16] C. Maraveas, Local Buckling of Steel Members Under Fire Conditions: A Review, Fire Technology, 55 (2019) 51-80.

[17] T. Ranawaka, M. Mahendran, Experimental study of the mechanical properties of light gauge cold-formed steels at elevated temperatures, Fire Safety Journal 44 (2) (2009) 219-229.

[18] B.W. Schafer, T. Peköz, Computational modelling of cold-formed steel: characterizing geometric imperfections and residual stresses, Journal of Constructional Steel Research 47 (3) (1998) 193-210.

[19] L. Gardner, R.B. Cruise, Modelling of residual stresses in structural stainless steel sections, Journal of Structural Engineering 135 (1) (2009) 42-53.

[20] K.J.R. Rasmussen, J. Rondal, Strength curves for metal columns, Journal of Structural Engineering 123 (6) (1997) 721-728.

[21] K.J.R. Rasmussen, J. Rondal, Column curves for stainless steel alloys, Journal of Constructional Steel Research 54 (1) (2000) 89-107.

[22] L. Gardner, Stability and design of stainless steel structures: Review and outlook, Thin-Walled Structures 141 (2019) 208-216.

[23] S. Afshan, L. Gardner, The continuous strength method for structural stainless steel design, Thin-Walled Structures 68 (2013) 42-49.

[24] EN 1993-1-2, Eurocode 3: Design of Steel Structures. Part 1–2: General Rules-Structural Fire Design, European Committee for Standardization, Brussels, Belgium, 2005.

[25] American Iron and Steel Institute (AISI). Specification for the cold-formed steel structural members. In: Cold-formed steel design manual, AISI S100, Washington, USA, 2007.

[26] M. V. A. Kumar, V. Kalyanaraman, Design strength of locally buckling stub-lipped channel columns, Journal of Structural Engineering 138 (11) (2012) 1291-1299.

[27] Standards Australia, AS/NZS 4673, Cold-formed Stainless Steel Structures, Sydney, Australia, 2001.

[28] K. J. R. Rasmussen, T. Burns, P. Bezkorovainy, Design of stiffened elements in cold-formed stainless steel sections, Journal of Structural Engineering 130 (11) (2004) 1764-1771.

[29] EN 1993-1-4, Eurocode 3: Design of Steel Structures. Part 1–4: General Rules-supplementary rules for stainless steels, European Committee for Standardization, Brussels, Belgium, 2006.

[30] G. Winter, Thin-walled structures-theoretical solutions and test results: Paper presented in Preliminary Publication of the 8th Congress, IABSE, Zurich, Switzerland, 1968.